A MICROSCOPIC DESCRIPTION OF NUCLEAR ALPHA DECAY

BY

OLUSEGUN G. OGUNBADE

Submitted in part fulfilment of the
requirements for the degree of

MASTER OF SCIENCE

in the subject

PHYSICS

at the

UNIVERSITY OF SOUTH AFRICA

SUPERVISOR: Dr. S. A. RAKITYANSKY

SEPTEMBER 2005

****

No one can comprehend what goes on under the sun. Despite all his efforts to search it out, man cannot discover its meaning. Even if a wise man claims he knows, he cannot really comprehend it.
Of making many books there is no end, and much study wearies the body. (Eccl. 8:17;12:12b)

DECLARATION

I declare that *A Microscopic Description of Nuclear Alpha Decay* is my own work and that all sources that I have used or quoted have been indicated and acknowledged by means of references.

Signed on this day, the ..... day of September 2005.

Candidate's signature

ACKNOWLEDGEMENTS

It is a pleasure to express my sincere gratitude to my supervisor **Dr. S. A. Rakityansky** for his help, guidance and unstinted support he has given me since the beginning of my studies with UNISA and especially during the compilation of this thesis—though this may sound like an alibi sentence to him, it never felt truer than with this thesis.

I take this opportunity to acknowledge all the input I have received from many of my enthusiatic colleagues in the department. I am especially indebted to Prof. M. Braun for his unswerving support in matters relating to Linux environment.

I also like to extend my heartfelt gratitude to my brother Dayo, my sister Yinka, my brother-in-law Dr. Matthew A. Dayomi and Naniso L. Teleki for their support and deadline reminder.

Hearty thanks go to our subject librarians Ms. Els ten Krooden and Tryphina Mokwetsi for their invaluable help and tirelessly updating me with materials used in completing this project.

My utmost gratitude goes to the Lord Almighty who has qualified me to share in the inheritance of the Physics community. Thank you Daddy, for the strength, perseverance and courage given me to make this work a success.

SUMMARY

Radioactive decay of nuclei via emission of α-particles is studied using three different theoretical approaches, viz: the quasi-bound state wavefunction approach (QSWA), the superasymmetric fission model (SAFM) and the semiclassical approximation (QCA). The half-lives of the radioactive nuclei, calculated using these methods, are compared with each other and with available experimental data.

The resonance wavefunction is obtained by numerically integrating the Schrödinger equation with outgoing boundary conditions. The sensitivity of the calculated decay widths to two particular parameter sets of the Woods-Saxon (WS) optical potentials are studied.

Double folding (DF) model calculations to obtain the bare α-nucleus potential have been carried out with the Reid M3Y effective nucleon-nucleon (NN) interactions. The exchange part of the interaction was taken to be of zero-range pseudo-potential and the density dependence of the NN interaction is accounted for.

The effectiveness of the method is demonstrated using both even-even and odd-mass spherical nuclei.

Keywords:

Alpha decay; Double folding potential; Superasymmetric fission model; Preformed cluster model; Optical potential; Quasi-bound wavefunction; Decay widths; Coulomb penetration factor; DDM3Y interactions; Gamow model.

Contents

Chapter 1

Introduction

The simplest view of the atomic nuclei is that they are composed of neutrons and protons, collectively called nucleons. Theoretical and experimental studies of nuclei revealed that the nucleons constituting them, are not distributed uniformly inside a nucleus. These studies proved the presence of "clusters" of nucleons in the nucleus, and the participation of such clusters in nuclear reactions. The concept of clustering is quite sophisticated and the definition of this will emerge later. Of all such clusters, the one formed by two protons and two neutrons is the most ubiquitous because of its high symmetry and binding energy. As is well known, this is referred to as the α-particle, although its properties inside a nucleus may not be the same as that of a free α-particle, owing to the action of the surrounding nucleons.

Some nuclei can spontaneously emit the α-particles. This phenomenon was discovered at the very beginning of the nuclear era and is known as the α-decay. There is a renewed interest in α-decay partly due to an increase of the role played by α-decay in the spectroscopy of unstable nuclei [1], which is primarily motivated by the connected question involving clustering of nucleons in nuclei [2] and partly due to "exotic" decay modes discovered in 1984 [3], which is decay via the spontaneous emission of heavier

clusters, such as ^{14}C, ^{20}O, ^{24}Ne, etc.

Alpha decay has been extensively studied over the years, and it has been found that calculations of relative half-lives give results in good agreement with the experimental values, but that it is far more difficult to account for the absolute values. One of the difficulties is that only one number (the half-life) is available experimentally; so it is not admissible to have even one adjustable parameter in the theory that is intended to explain the process. Everything must be calculated in terms of absolute values. In all models of alpha decay, the description of the process is either inseparably linked to the description of the nuclear reactions and quasi-stationary states [4] or as a superasymmetric fission, which may be conceived to be a sequence of adiabatic rearrangements, depicted as a continuous change of variables [5].

In what follows, we try to sketch out a historical background of the subject and describe the present status of the study of α-decay. Since this is a rich subject, neither completeness nor historical order is pursued. We focussed our attention to works that were done with the ambition of reproducing the absolute width, which is the touchstone for any microscopic description of the α-decay.

Historically, the theory of α-decay has developed through three stages. The first stage was characterized by a theoretical explanation of the global characteristics of the process: quantum mechanical barrier penetration. The emission of α-particles from some nuclei suggested that fully pre-formed α-particles exist in them, and their scarce appearance indicated that they are restrained by a potential barrier. This approach was independently and almost simultaneously given by Gamow [6] and by Condon and Gurney [7]. The half-life was determined by the penetrability of the barrier. The solution of this problem was one of the first successes of quantum mechanics. This stage was associated with the observation of the most intense (favored) α transitions. The second stage evolved as more alpha spectra called unfavored (or hindered) α transitions were identified. A description of such transitions became possible after the formulation of the shell model

and the R-matrix theory of nuclear reactions. In this model, α-decay involves two parts: the process of formation (structure part) and the process of penetration through the barrier (energy part). The probability of formation depends on the structure of nuclear states and determines the different classes of α transitions. In the original formulation of the R-matrix theory, the structure of the nucleus was little known and a black-box model was therefore proposed. Later, the description of the nuclear structure by single-particle or collective models constructed on the basis of an infinite oscillator potential constituted the third stage. In this way, the nucleus was assumed to be opaque. The use of such models makes it impossible to match correctly the interior and exterior wave functions.

In Gamow's treatment, the α-cluster was assumed to be a "particle" present in the nucleus from the outset, and the problem of clustering was not considered. Today we would say that this was a macroscopic theory. The Gamow theory reproduced the α-decay half-lives relative to each other in a range of many orders of magnitude, as is determined mostly by the decay energies. As an example of the large variation in the half-lives, consider the nucleus ^{213}Po which decays by emitting α-particles of energy 8.336 MeV has a half-life of 1.3×10^{-13} yr, whereas the half-life of ^{232}Th, which emits 3.98 MeV α-particles, is 1.4×10^{10} yr [8, 9]. These two cases, and many others in between, could nicely be fitted by the Gamow's model [10].

The great success of Gamow's theory was due to the excellent description of the penetration of the α-particle through the Coulomb barrier. It explained the linear relation between the logarithm of the decay width and the energy of the emitted particle (Q-value). The penetration probability is related to the half-life of the nucleus through the concept of the "frequency of escape attempts". That is, the α-particle was assumed to be moving as a little ball inside the nucleus bouncing on and reflected off the internal wall of the nuclear potential until it happens to 'tunnel' through the barrier. This semiclassical approach does not give allowance for the possibility that the emitted particle and/or the residual nucleus are not "pre-formed" in the parent. Thus it was later found that one

has to include a "pre-formation factor", which takes into account the probability that the mother nucleus is found in a state of the α-particle plus daughter nucleus. In spite of the pre-formation hypothesis, Gamow's intuitive model reproduces the experimental relative decay life-times (i.e. the ratios of different life-times) very well. This indicates that the pre-formation probability vary from case to case much less than barrier penetrabilities, but it does not allow to draw much more definite conclusions on the microscopic structure of nuclei.

At present few phenomelogical models based on this one-body formulation with different assumptions concerning the above two factors have been developed. Several phenomenological generalizations of the α-decay were essentially based on this idea. The most important is the preformed cluster model (PCM) of Buck *et al.* [11–14]. The PCM has been tried with various nuclear potentials e.g. square well [11], cosh-form [12, 13] and mixed Saxon-Woods form [14]. A smooth parametrization of this phenomenological potential, the effective α-core potential, enables one to satisfactorily predict all α-decay widths [13]. The decay width is obtained within the quasiclassical approximation (QCA) by following the procedure of Gurvitz and Kälbermann [15]. Buck and co-workers [11–14] within the framework of PCM successfully reproduced the experimental data of many nuclei. The theoretical half-lives from the cluster model agree with the data of the favored decays within a factor of $2 \sim 3$ [11–14].

The two main challenges in studies of α-decay were gradually recognised:

- The need to describe the behaviour of the nucleons which eventually constitute the α-particle both inside and outside the nucleus. This means that one has to describe simultaneously the behaviour of the nucleons both in the bound as well as in the unbound (continuum) state.

- The dynamics of these four bodies moving in the nuclear field pose an unsurmountable difficulty. The core of the problem is that the decay is a time-dependent

many-body processes. The decaying nucleus is a many-body wave packet, and the initial state is not even well defined.

A way to avoid solving the time-dependent many-body problem explicitly, was found with the introduction of nuclear reaction theory. It was understood that nuclear particles could penetrate through the nucleus and interact with its nucleons; there then appeared directions especially for the calculations of absolute widths of α-decay.

The dominant feature of reaction processes in which two nuclei collide to form a long-lived compound nucleus that subsequently disintegrates into a pair of nuclei, is the appearance of resonances [16]. Since the same compound system can be formed in different channels, the disintegration of the system is virtually independent of its birth. In this respect a compound resonance is reminiscent of a decaying state. Assuming that the reaction process is stationary and that the resonance that one is interested in is narrow, the collision matrix (or S-matrix), as a function of energy, can be parametrized in a many-level Breit-Wigner form [16], and the residues of the S-matrix are the partial decay widths. According to Lovas *et al.* [17], this resonance state corresponds to a pole of the S-matrix in the complex energy plane with a positive real part, or equivalently to the zero of the Jost functions. This is the complex eigenenergy belonging to the idealized decaying state i.e. it corresponds to the solution of the time-dependent Schrödinger equation with a time dependence of the form of $\exp[(-iE_n - \frac{1}{2}\Gamma_n)t/\hbar]$, which describes exponential decay, and can be valid only in a limited spatial region. (Otherwise the norm could not be constant in time [16].)

In the preceeding paragraph, it was assumed that the decaying state is stationary. The reason for the assumption is justified as follows: The half-lives of all α-emitters are very long indeed ($10^{-6} - 10^{17}$ s) in comparison with the "periods" of nucleon motions (10^{-21} s). Thus the average time before decay occurs is at least 10^{15} "nuclear periods" and may be as many as 10^{28}. In the time evolution of a decaying state the nucleus has many opportunities to establish a pattern of motion before it can actually disintegrate. Thus

the α-decay can be considered as a quasi-stationary process [9].

For the idealized decaying state, the eigenvalue problem $H\Psi = \mathcal{E}\Psi$, where $\mathcal{E} = E - i\frac{1}{2}\Gamma$, is to be solved, and the width is obtained from the resulting eigenenergy $\mathcal{E}$ as $\Gamma = -2\,\mathrm{Im}\,\mathcal{E}$. Among heavy nuclei, however, the values of Γ/E range between $10^{-10} - 10^{-30}$, therefore, such a procedure would require an enormous numerical difficulty [18]. The purpose of this study is, in part, to present ways to tackle this problem. Another objective is to describe a method that handles both the bound and resonant states as mentioned above on an equal footing and consequently avoid calculating the imaginary part of the resonant state position.

The first microscopic description of α-decay, published as late as in the fifties, was an application of a general theory of nuclear reactions, the R-matrix theory [19, 20]. This, combined with the shell model, which was formulated more or less at the same time, provided the basis of Mang's model [21] for α-decay. In the R-matrix formalism, to calculate these decay widths, we divide the configuration space of the compound system into two regions, the "internal region" V, to which the compound state is restricted, and the complementary "external region", which is the rest of the configuration space. All nuclear interactions among the nucleons that constitute the decaying α-particle and those in the daughter nucleus (including those induced by the Pauli principle) are only felt within the internal region. Therefore only the Coulomb interaction acting between the centres of mass of the fragments is important beyond V and in this external region the core and the emitted particle behave like a two-particle system moving outwards with asymptotic energy E_n. The solution inside the volume V satisfies a certain boundary condition on the surface S of V. In the decay of spherical nuclei the surface S can be chosen to be a sphere of radius R, where R is the distance between the centres of mass of the core and the emitted α-particle. The residues of the S-matrix can then be computed in terms of quantities evaluated on the surface S. One finds that the width

corresponding to the emission of a particle with angular momentum ℓ is given by [20].

$$\Gamma_\ell(R) = 2P_\ell(R)\gamma_\ell^2(R)\,, \tag{1.1}$$

where $P_\ell(R)$ is the Coulomb penetrability at distance R and $\gamma_\ell(R)$ is the reduced width, which is related to the formation amplitude $\mathcal{F}_\ell(R)$ at the point R by

$$\gamma_\ell(R) = \sqrt{\frac{\hbar^2 R}{2\mu}}\mathcal{F}_\ell(R)\,, \tag{1.2}$$

where μ is the reduced mass. The formation amplitude is the projection of the mother state onto the (antisymmetrized) product of the states of the two fragments.

The derivation of (1.1) was a great step forward in the study of alpha decay and it is the basis on which microscopic treatment of cluster decay is based. It contains all the elements of the Gamow theory plus another important ingredient, the preformation amplitude. The understanding of Coulomb penetrability is well known and has been excellently accounted for [22, 23]. The microscopic description of preformation factor has a key role in the understanding of the decay process and requires a precise knowledge of the initial quantum state. The success of this hinges in the ability to correctly match the outgoing wave (Gamow wave) with the internal wavefunction (α-particle formation amplitude) at a given radius near the touching configuration. There are several approaches to the calculation of the formation amplitude, the shell model [21], the hybrid (shell model + α-cluster) model [18], the BCS method [24] etc.

The application of the shell model to α-decay has a long record of numerous improvements in small steps [2, 21, 22, 25–31]. As was shown by Mang and Rasmussen, the shell model undershoots the decay width substantially [4, 21, 25]. The reason for this was found to be in the inconsistent way the Pauli effects were treated in the two-body description of the α-core motion [32]. This only affects calculations in which a macroscopic intercluster wave function is extrapolated into the range of the interfragment exchanges. For Thomas's formula (1.1) this means cases in which R was chosen within this range. A partial remedy was attained by Fliessbach and Mang [26], whose formalism allows us

to use radii within the range of Pauli exchanges.

The understanding of the role played by configuration mixing to induce the clustering of the four nucleons that would eventually constitute the α particle also posed a major problem within the shell approach. The importance of pairing correlations and configuration mixing was already realized in the early sixties [33, 34]. But their fundamental role in α-decay became clear only when large calculations were possible. Thus, it was found in Refs. [22, 27] that the inclusion of the neutron-neutron (n-n) and proton-proton (p-p) pairing interactions within a large shell-model configuration space to describe the movement of the α-particle inside the mother nucleus increases the calculated α-decay widths by several orders of magnitude for both spherical [22, 27] and deformed nuclei [35, 36]. The physics behind the enhancement induced by configuration mixing is that, with the participation of high-lying configurations, the pairing interaction clusters the two neutrons and the two protons on the nuclear surface [35, 37]. Yet, the eventual clustering of the α-particle is produced when the proton-neutron (p-n) interaction is also included [29]. The use of the cluster model to produce four-nucleon correlation on the nuclear surface was introduced by Wildermuth and co-workers [28, 38], and the concept of an "α giant resonance" to achieve the same phenomenology was proposed by Okabe [31].

Recently, Kaneko and Hasegawa [39] have shown that the nuclear correlations reveal themselves in the α-decay through the Q-value which affects the Coulomb penetrability. Furthermore, the "α-condensate" point of view suggests that the strong p-n correlations in $A > 208$ nuclei cause the α-like correlations. The α-like correlations are important for the penetration as well as the formation of α-particle. For these reasons, an accurate determination of the Q-value for α-decay process is paramount in our work.

The shell model is the most basic of all nuclear models, and any nuclear configuration can be described in terms of its basic states. This works very well for single-paricle (s.p.) states but becomes more difficult for cluster states. To describe a nucleus with an α-particle cluster requires the admixture of a large number of higher configurations. In

such cases, it is much simpler to represent the nucleus by a sum of shell-model and cluster configurations. The way to do this has been pioneered and described in detail by Tomoda and Arima [40]. In this model, called the extended shell-model, the wavefunctions of states below the α-particle threshold are described by the shell model, and those above by the cluster model. Tomoda and Arima made detailed calculations for ^{20}Ne and showed that it gives a good account of the energies, α-particle widths and $B(E2)$ values of the states of this nucleus. Tonozuka and Arima [22] extended this model to the study of surface α-clustering and α-decay of ^{212}Po. They included basis states up to $7\hbar\omega$ excitation quanta and went up perturbatively to $13\hbar\omega$. In order to treat such an immense function state, they neglected the p-n interactions and the two-particle states with two like nucleons occupying different orbits. Their value for absolute α-decay width was still small by a factor of 23, and with the inclusion of Fliessbach's prescription this was reduced to 14.

As already mentioned above, the inclusion of p-n correlation states in the ordinary shell model is a difficult task. The inclusion of the p-n interaction implies that the shell-model diagonalization is to be performed on a direct-product state space (i.e. a tensorial product space) of the two-neutron and two-proton bases. There are methods to deal with this problem. Among these, the multistep shell-model method (MSM) [41], which is based on a sophisticated truncation scheme, has the advantage that one describes the system in terms of previously calculated systems. Alpha-decay calculations in the framework of the MSM were presented in Ref [29]. The resulting decay width still falls short of the experimental value by a factor of ~ 15.

Most cluster-decaying nuclei have many valence nucleons, are deformed and some emit heavy clusters as well. Effort to develop a model of wide enough scope for these cases leads to the approach of Bardeen-Cooper-Schrieffer (BCS) theory, which is, generally, viewed as a shell-model based approximation scheme. It accounts for the most important correlations between nucleons outside closed shells in a reasonably good approximation. Technically, the BCS approach tranforms the wave function of a correlated system into

the form of a pure configuration. The BCS approach was introduced long ago in studying α-decay by Soloviev [34] and by Mang and Rasmussen [4, 25] and subsequently applied by Poggenburg *et al.* [42]. This approach was applied to the decay of deformed nuclei by these pioneers. The collective motions were described in the standard Bohr-Mottelson rotational model while the intrinsic motions were represented by BCS wave functions built up from Nilsson s.p. orbits expressed in terms of harmonic-oscillator wave functions. The penetration through the deformed potential barrier was describe in the WKB approximation.

These pioneering calculations were limited to very small basis sizes: they used single-shell valence spaces due to the limitation of computing facilities during the time.

Recently, the BCS treatment was applied to studying α-clustering in, and the α-decay of, spherical systems with many particles outside the core [30]. In that work the power of modern computers was exploited, and a large number of s.p. states were used. Later, the approach was used again for deformed nuclei [24, 36, 43, 44].

The first accurate calculation of an α-decay half-life was made by Varga *et al.* [18]. They made a detailed analysis of one of the simplest alpha decays, that of ^{212}Po to the the ground state of the doubly magic ^{208}Pb. Following Tomoda and Arima, they expressed the nuclear wavefunctions as the sum of a shell-model description of the ^{208}Pb core and a cluster-model description of the emitted α-particle. The cluster wavefunction is an antisymmetrized product of the intrinsic wavefunctions of the core nucleus, the emitted α-particle and of their relative motion. The decay was described by a Gamow wavefunction, which at large α-core distances becomes an outgoing Coulomb wave. The α-particle was described by 1s harmonic oscillator wavefunctions and the shell-model basis states obtained by diagonalizing the shell-model Hamiltonian. The calculation of the α-decay width was carried out avoiding the approximations inherent in previous work, and all the parameters were fixed from independent experimental data. They applied this formalism to calculate the absolute decay width of ^{212}Po, which decays to ^{208}Pb. This is a particularly favourable case, as the final nucleus has a double closed

shell. The result was $\Gamma = 1.45 \times 10^{-15}\,\mathrm{MeV}$, which agrees well with the experimental value of $\Gamma = 1.5 \times 10^{-15}\,\mathrm{MeV}$. The probability of formation of an α-particle inside the nucleus was found to be 0.3.

Further progress in the understanding of α-decay is associated with the development of non-R-matrix approaches, which in principle do not contain the arbitrary parameter R. The alternative approaches are based on one of the dynamical reaction theories. The formalism of Mang [4] as well as Harada and Rauscher [45] are based on the time-dependent perturbation theory, whereas the formalism of Kadmenskiĭ *et al.* [46] and of Schlitter [47] are based on a time-dependent and on a time-independent scattering theory of decay [48], respectively. Săndulescu *et al.* [49] resort to Feshbach's resonance theory based on the projector-operator techniques [50], while Jackson and Rhoades-Brown [51] provide several derivations for their decay-width formula, starting from different theories. Wildermuth *et al.* [38] use the unified resonating-group and shell-model theory of nuclei [52] to derive the Breit-Wigner formula, and from that the expression for the width.

Each theory introduces a bound initial state Ψ for the parent nucleus and a final scattering resonance state Φ. Most of the final results have essentially the same form, or indeed, are identical. The generic form of the decay-width formula is as follows:

$$\Gamma = 2\pi |\,\langle \Psi | H - H_0 | \Phi \rangle\,|^2\,, \tag{1.3}$$

where the Hamiltonians H_0 and H are associated with Ψ and Φ, respectively. The particular form depends on whether any of H_0 and H is an exact Hamiltonian and whether Ψ or Φ is taken to be an eigenstate of the corresponding Hamiltonian everywhere or just over a limited region.[‡]

In the fission-like model, various models have been proposed in the understanding of the highly asymmetric spontaneous disintegration of nuclei into two composite nuclear

[‡]Some of the approaches mentioned above, together with other approaches, are discussed in the review section of [51].

fragments e.g. involving α and various exotic decays had been predicted [53, 54]. These models can be broadly classified as the superasymmetric fission model (SAFM) [54–56] and the preformed cluster model (PCM) [57]. In the SAFM the barrier penetrabilities are calculated assuming two asymmetric clusters while in the PCM the cluster is assumed to be formed before it penetrates the barrier and its preformation probability is also included in the calculations.

In the SAFM, the most elegant phenomenological model has been formulated called the analytical superasymmetric fission model (ASAFM). The description of α-decay within this model reproduced the half-lives with reasonable success [55, 56]. In the ASAFM calculations, the entire interaction region is divided into two distinct zones. In the overlapping zone, where the distances of separation between the centres of the two fragments are below the touching radius, a parabolic form for the α-nucleus interaction potential has been used. And for distances beyond the touching radius only the Coulomb potential plus the centrifugal barrier for the separated fragments have been considered within a framework of a liquid drop model two center spherical parametrization.
Treating the region beyond the touching radius as a nuclear free-zone and approximating the nuclear interaction potential to a parabolic form in the overlapping region yield analytical expression for the WKB action integral [54]. Although the overall uncertainty of this ASAFM was found to be small, neither the division of the interaction region into two distinct domains is justifiable nor the use of parabolic nuclear potential has much physical basis.

Recently, microscopic description of α-nucleus interaction within the framework of SAFM has been carried out by Basu [58]. The microscopic nuclear potential is obtained by a double folding procedure of the densities of the fragments α and daughter nuclei with the finite range realistic Michigan 3 Yukawa (M3Y) effective interaction (DDM3Y) derived from the G-matrix elements. The density distribution functions for the α-particle and the daughter nucleus are chosen to be of Gaussian and spherical symmetric Saxon-Woods forms respectively. These, in turn are used to calculate the half-lives of the parent nuclei

for the α emission in the SAFM using the WKB approximation for the barrier penetration. The quantitative agreement with experimental data is excellent [58, 59]. The half-lives of the consecutive α-decay chains of the recently synthesized new superheavy element $^{287}115$ have been calculated within this formalism [59]. The results predict the general trend very well. The quantitative agreement is found to be reasonable [59].

The main objective of this thesis is to compare the reliability of new theories of alpha radioactivity. Below we undertake such a comparative calculation, using (i) the quasi-stationary decaying state approach, (ii) the superasymmetric fission model, and (iii) the one-dimensional semiclassical method. We demonstrate, numerically, the power and the weakness of the various procedures. The α-nucleus interactions needed for these calculations are obtained using both phenomelogical and microscopic approaches.

In Chapter 2 we shall describe the kinematics and characteristics of α-decay. The mathematical formalisms of some of the decay theories are briefly outlined in Chapter 3. In Chapter 4 a detailed description of the double folding model and the three different methods used in this work for calculating α-decay widths and half-lives are presented. In Chapter 5 the results are tabulated and discussed. Finally the conclusions of this work constituted the Chapter 6.

Chapter 2

Basic Equations and Conservation Laws

The majority of isotopes of the elements above and some neutron-deficient isotopes below Pb, decay by emission of α-particle. The α-decay process, which is described in various physics textbooks (see for example Ref. [60]), is the nuclear reaction

$$ {}^{A}_{Z}X \rightarrow {}^{A-4}_{Z-2}Y + \alpha \,, \tag{2.1} $$

where X and Y are known as the mother(parent) and daughter nuclei, respectively. Here, $\alpha \equiv {}^{4}_{2}\mathrm{He}$.

We assume that the decaying parent nucleus X is at rest. Then the energy of the initial system is just the rest energy of X, given as $M_X c^2$. The final state consists of Y and α, each of which will be in motion to conserve linear momentum. Thus the final total energy is $M_Y c^2 + T_Y + M_\alpha c^2 + T_\alpha$, where $T_i (i = \alpha, Y)$ represents the kinetic energy of the final fragments. Hence, conservation of energy requires that at infinitely large separation of the fragments

$$ M_X c^2 = M_Y c^2 + T_Y + M_\alpha c^2 + T_\alpha \,, \tag{2.2} $$

or

$$[M_X - M_Y - M_\alpha]c^2 = T_Y + T_\alpha \,. \tag{2.3}$$

The quantity on the left hand side of equation (2.3) is the net energy released in the decay, called the disintegration energy or the Q-value:

$$Q_\alpha = (M_X - M_Y - M_\alpha)c^2 \,. \tag{2.4}$$

Equation (2.4) represents the total amount of energy to be shared by the two final particles:

$$Q_\alpha = T_Y + T_\alpha \,. \tag{2.5}$$

An additional "screening correction" [25] to Q_α may be added to account for the influence of the electron cloud on the emitted α-particle

$$E_{scr} = +\left(65.3Z^{7/5} - 80Z^{2/5}\right) \text{ eV} \tag{2.6}$$

where Z is the proton number of the parent nucleus. This correction is at most around 47 keV (for $Z = 110$) and is often neglected.

Alternatively, the Q_α for α-decay of a nucleus $X(Z, N)$ can be obtained from the binding energies of the particles. It is given by the difference between the sum of the binding energies of the products of the decay and the binding energy of the decaying nucleus

$$Q_\alpha = B(Z-2, A-4) + B(2,4) - B(Z,A) \,. \tag{2.7}$$

where $B(2,4) \approx 28.3$ MeV is the binding energy of the α-particle.

A criterion for α instability emerges from these relations (2.4) and (2.7). From the energetics point of view, spontaneous α-emission is possible if $Q_\alpha > 0$. It is well known that the Q-values for nuclear α-decay rarely exceed 0.25 percent of the reduced mass, $\mu[= (M_\alpha \times M_Y)/(M_\alpha + M_Y)]$. Hence, nonrelativistic treatments are justified and usually employed. The above criterion i.e. $(Q_\alpha \geq 0)$ can only be satisfied if

$$B(2,4) > B(Z,A) - B(Z-2, A-4) \approx 4\frac{dB}{dA} = 4\left\{ A\frac{d(B/A)}{dA} + \frac{B}{A} \right\} . \tag{2.8}$$

It is well known that the inequality (2.8) is satisfied [60] when

$$\frac{B}{A} \leq 7.075 + 7.7 \times 10^{-3}\, A\,. \tag{2.9}$$

The angular momentum ℓ of the emerging α-particle also influences the decay process. This can be seen from the expression for the centrifugal barrier $[\hbar^2\ell(\ell+1)]/[2\mu r^2]$: higher values of ℓ increase the height of the barrier the α-particle must surmount. The possible values of ℓ for the outgoing α-particles are determined by the conservation of angular momentum and parity. Using the standard notations for the nuclear spins $\mathbf{I}_i$ and parities π_i $(i = X, Y)$ for the two nuclei of equation (2.1) along with the orbital angular momentum $\mathbf{L}$ for the α-daughter system. Since the α-particle has spin zero, conservation of angular momentum therefore results in the equality

$$\mathbf{I}_X = \mathbf{I}_Y + \mathbf{L}\,. \tag{2.10}$$

This constraint among quantized angular momentum vectors implies a condition on the associated quantum numbers. From the vector addition problem, the following bounds on the orbital angular momentum ℓ in terms of the initial and final spin quantum numbers is immediately established

$$|I_X - I_Y| \leq \ell \leq I_X + I_Y\,. \tag{2.11}$$

The nuclear states X and Y are also endowed with definite parities. The α-particle is known to have even parity and the final orbital parity is given by $(-1)^\ell$. Conservation of parity implies a multiplicative constraint among the various odd and even factors:

$$\pi_X = \pi_Y \cdot \pi_\alpha \cdot (-1)^\ell \tag{2.12}$$

where $\pi_\alpha = +$ is the parity of the α-particle.

In order to determine the lowest possible value of ℓ we classify the transitions into "parity-favored" and "parity-unfavored" decays. The results are listed in Table 2.1. Usually the α-decays occured between the ground states of even-even nuclei and between the states of odd-even nuclei and odd-odd nuclei with the same angular momentum and parity.

Table 2.1: Minimum value of L of the orbital angular momentum ℓ of the alpha particle in a transition $I_X, \Pi_X \rightarrow I_Y, \Pi_Y$

Parity-favored:	$\pi_X \pi_Y = (-1)^{I_X - I_Y}$	$\ell_{min} \equiv L = \lvert I_X - I_Y \rvert$
Parity-unfavored:	$\pi_X \pi_Y = (-1)^{I_X - I_Y + 1}$	$\ell_{min} \equiv L = \lvert I_X - I_Y \rvert + 1$
		provided that neither I_X nor I_Y is zero

This kind of decay is known as the favored α-decay because there is no change of the angular momentum and parity for the parent and daughter nuclei. If the state of the parent nucleus has different angular momentum and/or parity from that of the daughter nucleus, the decay is called the unfavored α-decay. Parity-unfavored transitions in which either I_X or I_Y or both are zero are absolutely forbidden by the conservation laws. Alpha-decays involving the ground states of even-even nuclei are presumably parity-favored, with $I_X = I_Y = 0$. It is imperative to know that that these decays would be completely forbidden if the parity conditions were unfavorable, i.e., if $\pi_X = -\pi_Y$. We conclude that ℓ must be even, to give even orbital parity, if X and Y have the same parity, and that ℓ must be odd if X and Y have the opposite parity.

The most remarkable feature of α-decay is the extraordinarily large variation in the half-life $T_{1/2}$ from one nuclide to another, while corresponding α-particle energies and Q-values vary within only a single order of magnitude. It is apparent that $T_{1/2}$ must have a very sensitive dependence on Q. The explanation for this behaviour is the basic reason for the development of different α-decay theories.

Part I

Review of α-decay theories

Chapter 3

Decay theories

In this chapter we present both the phenomenological and microscopic mathematical descriptions of some of the α-decay theories that have found practical applications and widely used over the years. Detailed descriptions of these methods can be found in the quoted references.

3.1 Phenomelogical models

3.1.1 Gamow Model

The simplest phenomenological model is the one-body model (Gamow model [6]), which assumes that the α-particles are already preformed in the nucleus. Correspondingly, the α-decay width $\Gamma_{\rm G}$ is given by the product between the frequency ν of the collision with the potential walls and the barrier penetrability P calculated using WKB approximation

$$\Gamma_{\rm G} = \nu P = \frac{v}{2R_i} \exp\left(-\frac{2}{\hbar}\int_{R_i}^{R_o} [2\mu(V(r)-Q)]^{1/2}\, dr\right) \tag{3.1}$$

where $v = (2Q/\mu)^{1/2}$, R_i and R_o are the inner and outer turning points, respectively, μ is the reduced mass and Q is the aymptotic energy of the relative motion. Alpha-decay studies with this model, using realistic potentials, have shown that the general trends of decay constants are well described, but not the absolute values. Consequently, a spectroscopic factor S was introduced which describes the preformation probability due to nuclear structure effects, as the ratio of the experimental decay width $\Gamma_{\rm exp}$ over the one-body decay width $\Gamma_{\rm G}$

$$\Gamma_{\rm exp} = S\Gamma_{\rm G} = S\nu P\,. \tag{3.2}$$

3.1.2 Preformed Cluster Model

Buck *et al.* [11–14] proposed an extreme cluster model of α-decay. By using a few parameters they successfully reproduced the experimental data of many nuclei [11–14].

The ground state of the parent nucleus in the cluster model is assumed to be an α-particle orbiting the daughter nucleus [11–14]. The orbit is denoted by a large value of the global quantum number $G = 2n + L$, where n is the node number of radial motion and L is the angular momentum [11–14]. The Bohr-Sommerfeld quantization is used to describe the motion of the α-particle in a given potential. It is assumed that the α-particle is preformed in the parent nucleus and therefore a preformed factor is introduced.

In the cluster model the α-core potential [11–14] is

$$V(r) = V_N(r) + V_C(r) + \frac{\hbar^2}{2\mu}\frac{(L+\frac{1}{2})^2}{r^2}\,, \tag{3.3}$$

where the nuclear potential $V_N(r)$ is given in various forms e.g. square well [11], cosh-form [12, 13] and mixed Saxon-Woods form [14]. The "cosh" geometry of depth V_0, diffuseness a, and radius R_n is given by the relation

$$V_N(r) = -V_0\frac{1+\cosh(R_n/a)}{\cosh(r/a)+\cosh(R_n/a)} \tag{3.4}$$

and the Coulomb potential is taken to be of a spherical charge distribution (SCD) of radius R_c (usually, $R_c = R_n$)

$$\begin{aligned} V_C(r) &= \frac{Z_\alpha Z_d e^2}{r} && \text{for } (r \geq R_c), \\ &= \frac{Z_\alpha Z_d e^2}{2R_c}\left[3 - \left(\frac{r}{R_c}\right)^2\right] && \text{for } (r \leq R_c)\,, \end{aligned} \tag{3.5}$$

where Z_α and Z_d are the charges of the α-particle and the core, respectively. A Langer modified centrifugal barrier is used with $L(L+1)$ replaced by $(L+\frac{1}{2})^2$.

There are three classical turning points for the above potentials and they are denoted as r_1, r_2 and r_3 in order of increasing distance from the origin. Their values are obtained by numerical solutions of the equation $V(r) = Q$, where Q is the energy appropriate to the decay under consideration. The value of Q is deduced from the measured α-particle kinetic energy by applying a standard recoil correction, as well as an electron shielding correction in a systematic manner as given by equation (2.6) in Chapter 2. Hence,

$$Q = \frac{A_p}{A_p - 4}E_\alpha + (65.3Z_p^{7/5} - 80.0Z_p^{2/5})10^{-6}\,\text{MeV}, \tag{3.6}$$

where Z_p and A_p are the charge and mass numbers, respectively, of the parent nucleus. The radius parameter R can be determined separately for each decay by applying the Bohr-Sommerfeld quantization condition:

$$\int_{r_1}^{r_2} dr \sqrt{\frac{2\mu}{\hbar^2}[Q - V_N(r) - V_C(r)] - \frac{(L+\frac{1}{2})}{r^2}} = (2n+1)\frac{\pi}{2} = (G - L + 1)\frac{\pi}{2}\,. \tag{3.7}$$

In semiclassical approximation, the α-decay width Γ [11–14] is given by

$$\Gamma = PF\frac{\hbar^2}{4\mu}\exp\left[-2\int_{r_2}^{r_3} k(r)\,dr\right]. \tag{3.8}$$

The normalization factor F is

$$F\int_{r_1}^{r_2} dr \frac{1}{k(r)}\cos^2\left(\int_{r_1}^{r} dr' k(r') - \frac{\pi}{4}\right) = 1\,, \tag{3.9}$$

where the squared cosine term may be replaced by $\frac{1}{2}$ without significant loss of accuracy, so that

$$F\int_{r_1}^{r_2} \frac{dr}{2k(r)} = 1\,, \tag{3.10}$$

with the wave number $k(r)$ given by

$$k(r) = \sqrt{\frac{2\mu}{\hbar^2} \mid Q - V(r) \mid}. \tag{3.11}$$

The α-decay half-life $T_{1/2}$ is then related to the width by

$$T_{1/2} = \frac{\hbar \ln 2}{\Gamma}. \tag{3.12}$$

Buck *et al.* [11–14] obtained the values of the parameters in the above potential by fitting the available data on elastic scattering of favored α-particle from nuclei. They are $V_0 = 162.3\,\mathrm{MeV}$ and $a = 0.40\,\mathrm{fm}$. The preformation factor of the α cluster is chosen to be $P_\alpha = 1.0$ for even-even nuclei, $P_\alpha = 0.6$ for odd-A nuclei, $P_\alpha = 0.35$ for odd-odd nuclei. The values of the global quantum numbers are

$$\begin{aligned} G &= 22 \qquad \text{for} \quad N > 126, \\ G &= 20 \qquad \text{for} \quad 82 < N \leqslant 126, \\ G &= 18 \qquad \text{for} \quad N \leqslant 82, \end{aligned} \tag{3.13}$$

where N is the parent nucleus neutron number.

3.2 Microscopic Models

The touchstone of all microscopic theories of α-decay is to reproduce the absolute decay width. It is well known that the decay is a surface phenomenon, while the usual microscopic theories of nuclear structure only provide reliable description for the nuclear interior.

3.2.1 Self-Consistent Microscopic Approach

In what follows we shall briefly, for convenience, recall the standard microscopic approach (SMA) to compute the α-decay width for spherical nuclei.[†] The full exposition of this

[†]It was shown in [43] that for normal deformations 90% of the effect is given by the Coulomb barrier.

method can be found in great number of articles (see e.g., [4, 17]).

As we mentioned in the introduction, the narrow resonance behaves almost like a bound state with real energy. The wavefunction has a strongly decreasing behaviour inside the barrier and can be normalized to unity in the internal region. In order to ensure the continuity, the external outgoing spherical Coulomb wave should be multiplied by some coefficient. It turns out from the continuity that this matching coefficient squared is proportional to the decay width, or to the inverse half-life. Following the continuity equation, the decay width is given by the relation

$$\Gamma \equiv \sum_{\ell} \Gamma_{\ell} = \lim_{r\to\infty} \hbar v \sum_{\ell} |g_{\ell}(r)|^2 \,, \tag{3.14}$$

where v is the relative velocity between the emitted cluster and daughter nucleus. The radial multipole component of the wavefunction is a spherical wave of the form $g_{\ell}(r)/r$. In the external region, beyond the touching configuration, the function g_{ℓ} obeys a stationary Schrödinger equation

$$\frac{\hbar^2}{2\mu}\left[-\frac{d^2}{dr^2} + \frac{\ell(\ell+1)}{r^2}\right] g_{\ell}(r) + V(r) g_{\ell}(r) = E\, g_{\ell}(r)\,. \tag{3.15}$$

This equation can be integrated backwards (in the stable direction) starting from large distances, where $V(r)$ becomes a purely Coulomb potential and the solution is a spherical outgoing wave

$$\lim_{r\to\infty}[g_{\ell}(r)] = C_{\ell}[G_{\ell}(kr) + iF_{\ell}(kr)] \tag{3.16}$$

where k is a complex momentum. As already pointed out, a narrow resonance has a small imaginary part of E and consequently the regular Coulomb functions $F_{\ell}(kr)$ have vanishing values inside the barrier. Therefore, the constants C_{ℓ} are practically real numbers and $|E| = Q$. These numbers are determined by matching the outgoing wave (3.16) with the internal solution at a given radius R near the touching configuration

$$\frac{g_{\ell}(R)}{R} = \mathcal{F}_{\ell}(R)\,. \tag{3.17}$$

Here $\mathcal{F}_{\ell}$ is the ℓth multipole component of the α-cluster formation amplitude. Taking into account that $\lim_{r\to\infty} |G_{\ell}(kr) + iF_{\ell}(kr)| = 1$ one obtains from equations (3.14) and

(3.16) that the decay width is proportional to the matching coefficient squared, i.e.

$$\Gamma_\ell = \hbar v \, |C_\ell|^2 \, . \tag{3.18}$$

By using equation (3.17) this relation can be written as follows:

$$\Gamma_\ell = \hbar v \left[\frac{R\mathcal{F}_\ell(R)}{G_\ell(kR)} \right]^2 \equiv P_\ell \, \gamma_\ell^2 \tag{3.19}$$

where we use the well-known factorization in terms of the penetrability and reduced width, respectively

$$P_\ell = \frac{2kR}{G_\ell^2(kR)} \qquad \gamma_\ell = \left[\frac{\hbar^2}{2\mu} \right]^{\frac{1}{2}} R^{\frac{1}{2}} \mathcal{F}_\ell \, . \tag{3.20}$$

The last equality in (3.19) is the standard formula used for many years to estimate α-decay widths [19]. The generalization for deformed nuclei within the coupled channel approach is described in [61].

Delion and Săndulescu [62] have shown that the matching condition (3.17) should in general refer to the logarithmic derivative which is expressed in the form

$$f_\ell(R) \equiv \frac{g'_\ell(R)}{g_\ell(R)} = \frac{[R\mathcal{F}_\ell(R)]'}{R\mathcal{F}_\ell(R)} = \frac{G'_\ell(kR)}{G_\ell(kR)} \, . \tag{3.21}$$

It is easily seen that this is equivalent to the standard condition for a resonant state: the phase shift defined by [62]

$$\lim_{r\to\infty} [g_\ell(r)] = C_\ell [G_\ell(kr) \sin\delta_\ell + i F_\ell(kr) \cos\delta_\ell] \tag{3.22}$$

where k is a real momentum and has a sharp change by passing through $\delta_\ell = \pi/2$. For this value the matching condition (3.21) (concerning only the irregular Coulomb function) is fulfilled. The irregular Coulomb wave function is strongly dependent on the Q-value therefore, the microscopic formation amplitude entering condition (3.21) should follow this dependence.

The microscopic cluster formation amplitude (CFA) entering equation (3.17) for α-decay process is defined by the following overlap integral

$$\mathcal{F}_\ell(R) = \iiint [\Psi_\alpha(\xi_\alpha)\Psi_A(\xi_A)Y_{\ell 0}(\hat{R})]^* \Psi_B(\xi_B) \, \mathrm{d}\xi_\alpha \, \mathrm{d}\xi_A \, \mathrm{d}\hat{R} \tag{3.23}$$

where ξ denotes the internal coordinates and R the centre of mass (cm) coordinate. The α-daughter antisymmetrization can be neglected if the radius R is larger than the touching radius R_c.

The details of how to estimate integral (3.23) are given in [44]. We mention here that the most important ingredients are the single particle (sp) proton and neutron eigenfunctions. They are obtained by using the harmonic oscillator (ho) diagolinalization basis with a standard procedure

$$b = \frac{M_0\omega}{\hbar} \qquad \hbar\omega = 41\, A^{-1/3} \tag{3.24}$$

where M_0 is the nucleonic mass. By changing the proton and neutron coordinates to the relative and cm cooridinates one can analytically compute the overlap integral (3.23) in terms of Talmi-Moshinsky brackets.
In order to have a proper asymptotic behaviour at large distances (beyond the touching configuration) it is necessary to include a large number of spherical shells in the basis. But this can also be achieved by using a mixed non-orthogonal ho basis, thus reducing the number of shells. For this purpose, Delion *et al.* [63] gave a more general representation in terms of radial ho wavefunctions

$$u_\ell(r) = \sum_{2n_1+\ell=N_1\leqslant N_0} c^{(1)}_{n_1\ell}\mathcal{R}^{(b_1)}_{n_1\ell}(r) + \sum_{2n_2+\ell=N_2>N_0} c^{(2)}_{n_2\ell}\mathcal{R}^{(b_2)}_{n_2\ell}(r)\,. \tag{3.25}$$

Here b_1 is the ho parameter corresponding to a potential which fits the Wood-Saxon interaction in the region of the discrete spectrum. On the other hand, a smaller b_2 corresponds to a flatter ho potential that describes better the continuum part of the spectrum as a quasicontinuum. These parameters are connected with the standard ho parameter (3.24) by the multiplier f_k,

$$b_k = f_k b \qquad k = 1,\, 2\,. \tag{3.26}$$

Here equation (3.25) is an 'effective' representation of the continuum, consistent with the used two-body residual interaction and the parameter b_2 is chosen in such a way so as to obtain a minimal amount of basis states reproducing the decay width.

3.2.2 Microscopic Approach with Optical Model

Another simple microscopic decay theory (MAOM) was developed in [64], by extending the basic formalism of [49] which unifies the advantages of the shell-model description of nuclei involved with the optical model for the emitted cluster. This microscopic description of the decay needs to know two sets of basic states: the states $|\Phi_K\rangle$ of the initial system and the scattering states $|\Phi_E^C\rangle$ describing the relative motion in the final channel.

If the states $|\Phi_K\rangle$ are approximated with the bound-shell model or the quasibound [64] wavefunctions (in these cases K denotes a set of discrete quantum numbers), the scattering states may be obtained by solving the integral equation

$$(E - H)|\chi_E^C\rangle = \sum_K \langle \phi_K \mid H \mid \chi_E^C \rangle |\phi_K\rangle \tag{3.27}$$

where H is the Hamiltonian of the system, E is the total energy and C is the channel index.

Equation (3.27), together with the orthogonality condition,

$$\langle \phi_K \mid \chi_E^C \rangle \tag{3.28}$$

determine the decay width of the state

$$\Gamma_K = 2\pi \sum_C |\langle \phi_K \mid H \mid \chi_E^C \rangle|^2 . \tag{3.29}$$

The general solution of equation (3.27) may be written as

$$|\chi_E^C\rangle = |\chi_{E,0}^C\rangle - \sum_K \langle \phi_K \mid H \mid \chi_E^C \rangle |\chi_{E,K}^C\rangle \tag{3.30}$$

where $|\chi_{E,i}^C\rangle$ $(i = 0, K)$ are solutions of the homogeneous and inhomogeneous equations

$$(E - H) \left\{ \begin{array}{c} |\chi_{E,0}^C\rangle \\ |\chi_{E,K}^C\rangle \end{array} \right\} = \left\{ \begin{array}{c} 0 \\ |\phi_K\rangle \end{array} \right\} . \tag{3.31}$$

Using equations (3.28) and (3.30) in equation (3.29), one obtains for the width of one level

$$\Gamma_K = 2\pi \sum_C \left| \frac{\langle \phi_K \mid \chi^C_{E,0} \rangle}{\langle \phi_K \mid \chi^C_{E,K} \rangle} \right|^2 = \sum_C \Gamma_{CK} \,. \tag{3.32}$$

The partial width Γ_{CK} can be reduced to the radial dependence by using a model Hamiltonian for the final state

$$H = H_{A-N} + H_N + V_{A-N,N} \,, \tag{3.33}$$

where H_{A-N} and H_N are Hamiltonians containing only the internal coordinates of the fragments, and $V_{A-N,N}$ represents the kinetic and potential energies in the relative coordinate.

In the channel region a similar seperation is performed for the wavefunctions $|\chi^C_{E,0}\rangle$ and $|\chi^C_{E,K}\rangle$ and energy

$$|\chi^C_{E,0}\rangle = \phi^0_C(r)[|\phi_{A-N}\rangle|\phi_N\rangle|\gamma_{LM}\rangle] \tag{3.34}$$

$$|\chi^C_{E,K}\rangle = \phi^K_C(r)[|\phi_{A-N}\rangle|\phi_N\rangle|\gamma_{LM}\rangle] \tag{3.35}$$

$$E_A = E_{A-N} + E_N + \varepsilon \tag{3.36}$$

where ϕ^i_C $(i = 0, K)$ are solutions for the relative motion of the energy E that will be determined, and ϕ_{A-N}, E_{A-N} and ϕ_N, E_N are the internal wavefunctions and energies of the fragments, respectively.

Equations for the relative wavefunctions result by projecting equations (3.31) and (3.29) on the channel wavefunctions $[|\phi_{A-N}\rangle|\phi_N\rangle|\gamma_{LM}\rangle]$:

$$[T_{A-N,N}(r) + V_{A-N,N}(r) - \varepsilon] \left\{ \begin{array}{c} \phi^0_C(r) \\ \phi^K_C(r) \end{array} \right\} = \left\{ \begin{array}{c} 0 \\ \mathcal{F}^K_C(r) \end{array} \right\} . \tag{3.37}$$

where the projection of the initial state $|\phi_K\rangle$ (on the channel wavefunction) is the cluster formation amplitude (CFA)

$$\mathcal{F}^K_C(r) = r\langle \phi_K | [|\phi_{A-N}\rangle|\phi_N\rangle|\gamma_{LM}(r)\rangle] \rangle \,. \tag{3.38}$$

Finally, using in equation (3.29) equations (3.34), (3.35) and (3.38), one obtains

$$\Gamma_{CK} = 2\pi \left| \frac{\langle \mathcal{F}_C^K(r) \mid \phi_C^0(r) \rangle}{\langle \mathcal{F}_C^K(r) \mid \phi_C^K(r) \rangle} \right|^2 . \tag{3.39}$$

It should be noted that no channel radius was introduced in this formulation of α-decay.

The microscopic treatment of the emission rates starts with the calculation of the basic states $|\phi_K\rangle$ by diagonalizing a shell-model Hamiltonian in a truncated space, after which the CFA is constructed from the orbitals outside the closed shells. After calculating the CFA with the energy released and the potential interaction in the final state, the differential equations (3.37) are solved numerically with the usual boundary conditions for the scattering states (incoming waves in channel C and outgoing waves in all open channels). No antisymmetry in the final channel is introduced. With such a simple theory, the experimental α-decay half-lives are quite nicely reproduced [64].

3.2.3 Microscopic description and Superasymmetric Fission Model

The method of calculating α-decay half-lives based on the double folding and SAFM models for the spherical [58, 65] and superheavy [59, 66] nuclei is presented in this section. The calculated densities along with the energy and realisitc M3Y effective nucleon-nucleon interaction is used in the double folding model to compute the respective interaction energies between the α-daughter system (see Chapter 4) . These, in turn are used to calculate the half-lives of the parent nuclei for the α emission in the SAFM using the WKB approximation.

The total interaction energy $V(r)$ between the α nucleus and the residual daughter nucleus is equal to the sum of the nuclear interaction energy, the Coulomb interaction energy and the centrifugal barrier. Thus

$$V(r) = V_N(r) + V_C(r) + \frac{\hbar^2}{2\mu} \frac{\ell(\ell+1)}{r^2} , \tag{3.40}$$

where $\mu = mA_\alpha A_d/A$ is the reduced mass, A is the mass number of the parent nucleus and m is the nucleon mass measured in units of MeV/c^2. The minimum centrifugal barrier is determined from the spin parity conservation as shown in Chapter 2.

The α-nucleus Coulomb interaction potential $V_C(r)$ is either assumed to be of a point charge distribution (PCD) $Z_\alpha Z_d e^2/r$ for all r or as a SCD (see equation (3.5)). The touching radial separation R_c between the α-particle and the daughter nucleus is given by $R_c = c_\alpha + c_d$ where c_α and c_d are obtained from equation (4.18). Although a more realistic form of $V_C(r)$ can be obtained from DFM equation (4.2), both the PCD and SCD are sufficient for most cases in α-particles decay. The α-nucleus nuclear potential $V_N(r)$ is given by equation (4.25). The energy E that appears in equation (4.25) is the energy measured in the centre of mass of the α-decay nucleus system which is equal to the released energy Q.

The half-life $T_{1/2}$ of the parent nucleus against its split into an α and a daughter in the SAFM is given

$$T_{1/2} = \frac{h \ln 2}{2E_v}(1 + e^K)\,, \tag{3.41}$$

where, within the WKB approximation, the action integral K of equation (3.41) is given by

$$K = \frac{2}{\hbar}\int_{r_a}^{r_b} \{2\mu[V(r) - E_v - Q]\}^{1/2}\, dr \tag{3.42}$$

where r_a and r_b are the inner and outer turning points, respectively, determined from the equations

$$V(r_a) = Q + E_v = V(r_b)\,. \tag{3.43}$$

The Q value for the α-decay can be obtained either from the kinetic energy (corrected for the recoil) see eq. (3.6) or from the binding energies of the α nuclei, daughter nuclei and the parent nuclei. $E_v(= 1/2\hbar\omega = 1/2hv)$ is the zero point vibrational energy, where v is the assualt frequency, and is the parameter appearing in SAFM. The zero point vibration energies for the α decays which include the shell and pairing effects are given

as

$$\begin{aligned} E_v &= 0.1045\,Q \qquad \text{for} \quad \text{even(Z) – even(N) parent nuclei} \\ &= 0.0962\,Q \qquad \text{for} \quad \text{odd(Z) – even(N) parent nuclei} \\ &= 0.0907\,Q \qquad \text{for} \quad \text{even(Z) – odd(N) parent nuclei} \\ &= 0.0767\,Q \qquad \text{for} \quad \text{odd(Z) – odd(N) parent nuclei} \end{aligned} \tag{3.44}$$

The results of the calculations using M3Y and DDM3Y supplemented by a pseudo-potential are in excellent agreement over a wide range of experimental observed data spanning about thirty-five orders of magnitude [58].

Part II

Our calculations

Chapter 4

Methods of Calculation

As already mentioned in Chapter 1, since the α resonances are extremely narrow and correspond to half-lives that vary over a wide range $\sim 10^{-6} - 10^{17}$ s, it is difficult to localize the corresponding S-matrix poles numerically. Therefore, in our work, for calculating Γ we shall use three different methods based on three theoretical models described in Chapter 3. Our choice of the models is determined purely on the ground of numerical computation and conveniency. The methods are labeled as Methods A, B and C:

Method A. The quasi-bound state wave function approach (QSWA).

Method B. The superasymmetric fission model, SAFM and DFM.

Method C. The quasiclassical approximation, QCA and DFM.

The SAFM and QCA have been described in section 3.2.3 and section 3.1.2, respectively. The QSWA method is described below.

To keep our calculations concise and simple, we apply the above methods to the region of nuclei for α-decays which proceed 100% to the daughter ground state, with the exception

of ^{217}Th, and for which the spins of both the initial and final states are known. We compare our alpha decay half-lives calculations with measured values for 13 even-even nuclei and three odd-mass nuclei. We have restricted attention to mostly even-even parent nuclei for two main reasons. On the one hand, we can be sure that we are dealing with pure $L = 0$ transitions. On the other hand, the ground state of the daughter nucleus is always the most populated following the decay, and is a natural candidate for the core in the DFM model. Both these simplifications are absent when considering the decays of odd-mass nuclei. To this end, we carefully chose the odd-A decay data to include in our set. Furthermore, we also use the odd-mass parent nuclei to test the extent of application of our theoretical models. In addition, from the WKB action integral, it is known that the barrier penetration depends exponentially on the Q-value, therefore we chose data whose experimental ground state masses are accurately known for correct determination of the Q-value.

In Table 4.1, we show all the parent nuclei for which we made calculations and the data used. We chose a sample of 16 α emitting nuclei, in different regions of the periodic table, for which reliable data exist. The radial quantum number N is guessed by following the procedure given by Wildermuth et al. [74] for the ground state to ground state transitions. The choice of the global quantum number G and minimum angular momentum l_{min} are as described in section 3.1.2 and Chapter 2. The experimental data $T_{1/2}^{expt}$ are taken from reference [56].

We now describe the double folding potential formalism since it plays a central and crucial role in the methods we are using in this work.

4.1 The Double Folding Model

The double folding model (DFM) was applied to calculate the nucleus-nucleus potential. This interaction is based upon a realistic G-matrix [67]. This model has been widely used

Table 4.1: Alpha decay data used in our calculation. The nuclear spin J^π of the parent and daughter nuclei has been added.

System	J^π	N	G	l_{min}	$T_{1/2}^{expt}$(s)
^{144}Nd $\rightarrow$ ^{140}Ce + α	(0+,0+)	10	18	0	(7.222±0.505)×10^{22}
^{146}Sm $\rightarrow$ ^{142}Nd + α	(0+,0+)	10	18	0	(3.248±0.158)×10^{15}
^{150}Gd $\rightarrow$ ^{146}Sm + α	(0+,0+)	11	18	0	(5.645±0.252)×10^{13}
^{152}Gd $\rightarrow$ ^{148}Sm + α	(0+,0+)	11	18	0	(3.406±0.252)×10^{21}
^{174}Hf $\rightarrow$ ^{170}Yb + α	(0+,0+)	11	18	0	(6.307±1.261)×10^{22}
^{190}Pt $\rightarrow$ ^{186}Os + α	(0+,0+)	11	18	0	(2.050±0.095)×10^{19}
^{208}Po $\rightarrow$ ^{204}Pb + α	(0+,0+)	12	20	0	(9.139±0.006)×10^{7}
^{212}Pb $\rightarrow$ ^{208}Po + α	(0+,0+)	11	22	0	(2.990±0.020)×10^{-7}
^{216}Rn $\rightarrow$ ^{212}Po + α	(0+,0+)	12	22	0	(4.500±0.020)×10^{-5}
^{224}Ra $\rightarrow$ ^{220}Rn + α	(0+,0+)	12	22	0	(3.162±0.020)×10^{5}
^{232}Th $\rightarrow$ ^{228}Ra + α	(0+,0+)	12	22	0	(4.431±0.020)×10^{17}
^{240}Cm $\rightarrow$ ^{236}Pu + α	(0+,0+)	12	22	0	(2.345±0.020)×10^{6}
^{256}Fm $\rightarrow$ ^{252}Cf + α	(0+,0+)	12	22	0	(1.167±0.020)×10^{5}
^{217}Th $\rightarrow$ ^{213}Ra + α	(9/2+,1/2-)	12	22	5	(2.520±0.020)×10^{-4}
^{227}Ac $\rightarrow$ ^{223}Fr + α	(3/2-,3/2-)	12	22	0	(4.975±0.003)×10^{10}
^{229}U $\rightarrow$ ^{225}Th + α	(3/2+,3/2+)	12	22	0	(1.740±0.020)×10^{4}

in the last 20 years to calculate the first-order term of the real part of the microscopic optical potential for elastic and inelastic scattering of α-particles and heavy ions [68]. In practice, the strength of the DFM potential is often renormalized by a factor (expected to be greater than unity) to give the best fit to experimental scattering data. This factor is attributed to the higher-order terms which cannot be calculated with the DFM. Although detailed descriptions of the DFM can be found in many papers (see, e.g., Refs [69, 70]), in order to make this work self-contained we present in the next section a short description of the main formulae and parameters used.

4.1.1 Formalism of the DFM

The interaction potential between two nuclei is, generally, written as

$$U(R) = U_C(R) + U_N(R) + U_{rot}(R), \tag{4.1}$$

where U_C is due to the electrostatic (Coulomb) interaction, U_N is the strong (nuclear) interaction, and U_{rot} is the rotational term. This last term has a very simple structure, and since the barriers required for α-decay is provided by the Coulomb barrier, it will not be considered here.

The Coulomb energy for two spherical nuclei can be written as

$$U_C(R) = \int d\mathbf{r}_1 \int d\mathbf{r}_2 \rho_{1ch}(\mathbf{r}_1) v_C(\mathbf{s}) \rho_{2ch}(\mathbf{r}_2). \tag{4.2}$$

Here ρ_{1ch} and ρ_{2ch} are the charge densities of the two interacting nuclear fragments i.e. α-particle and daughter nuclei, and v_C is the Coulomb interaction. The vector $\mathbf{s} = \mathbf{R} + \mathbf{r_2} - \mathbf{r_1}$ corresponds to the distance between two interacting points of the α-particle and daughter nucleus, whose radius vectors are $\mathbf{r_1}$ and $\mathbf{r_2}$, respectively. $\mathbf{R}$ denotes the vector joining the centers of mass of the two nuclei. This geometry is illustrated in Fig. 4.1. The nuclear part of the potential, U_N, consists of two terms, the direct U_{ND} term and the exchange U_{NE} term, which are generally energy dependent. The exchange term is introduced to properly account for the antisymmetrization of the individual internal wavefunctions under the interchange of nucleons between the two interacting nucleons. Interchanging the spatial positions of the two nucleons affects the position of the centres of mass of the two nuclei. The corresponding exchange contribution U_{NE} to the potential becomes nonlocal. The direct part of the interaction between two colliding nuclei has a similar form to the equation describing the Coulomb interaction:

$$U_{ND}(R, E) = g(E) \int d\mathbf{r}_1 \int d\mathbf{r}_2 \rho_{1A}(\mathbf{r}_1) v_D(\mathbf{s}) \rho_{2A}(\mathbf{r}_2). \tag{4.3}$$

Here ρ_{1A} and ρ_{2A} are the nucleon densities of the colliding nuclei, v_D is the direct part of the nuclear interaction between two nucleons (NN interaction), and $g(E)$ is a multiplier

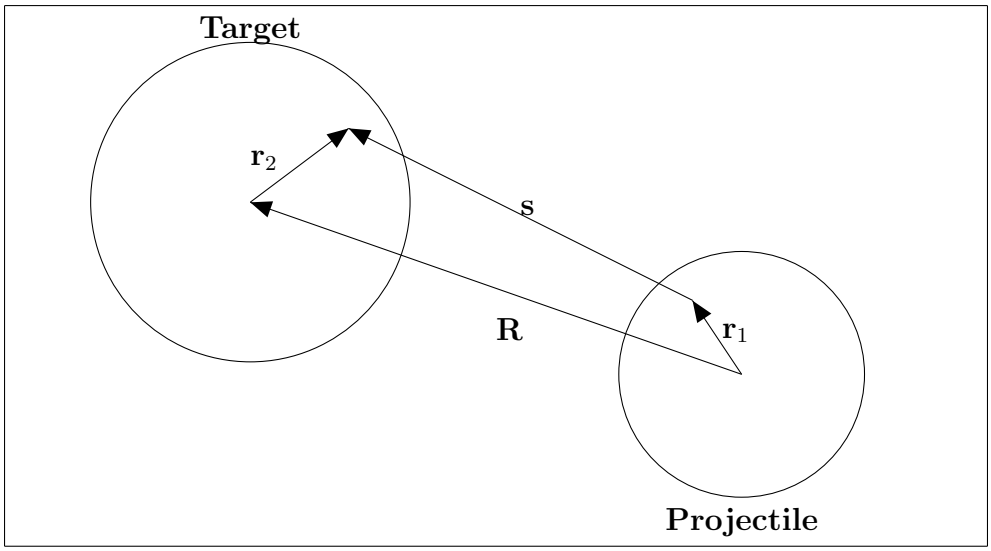

Figure 4.1: Geometric parameters for the Double Folding Potential.

that depends upon the energy per nucleon mass $E = E_{lab}/A_P$. The exchange part involves nondiagonal elements of the density matrix [69]:

$$U_{NE}(R,E) = g(E) \int d\mathbf{r}_1 \int d\mathbf{r}_2 \rho_{1A}(\mathbf{r}_1;\mathbf{r}_1+\mathbf{s}) v_E(\mathbf{s}) \rho_{2A}(\mathbf{r}_2;\mathbf{r}_2-\mathbf{s}) exp(i\mathbf{ks}/\mu). \quad (4.4)$$

The wave number k associated with the relative motion of the colliding nuclei is given by

$$k^2(R) = \frac{2\mu}{\hbar^2}[E_{c.m.} - U(R)], \quad (4.5)$$

where the reduced mass number $\mu = A_1 A_2 m_n/(A_1 + A_2)$, and m_n is the bare nucleon mass.

Two parametrizations of the nucleon-nucleon interaction in the literature are based, respectively, on the Reid and Paris [67, 69] interactions. These comprise a sum of Yukawa-type terms, known as M3Y effective nucleon-nucleon interactions, comprising both direct

v_D and exchange v_E terms:

$$v_D(s) = \sum_{i=1}^{3} G_{Di}[exp(-s/r_i)]/(s/r_i)\,, \tag{4.6}$$

$$v_E(s) = \sum_{i=1}^{3} G_{Ei}[exp(-s/r_i)]/(s/r_i)\,. \tag{4.7}$$

Here subscript D refers to the direct part of NN interaction and the subscript E refers to the finite-range exchange part of the NN interaction. Each term is determined by the radius parameters r_i and the coefficient G_{Di} and G_{Ei}. Instead of a finite-range exchange NN interaction, one of zero-range was used in early works [68]:

$$v_{E\delta}(\mathbf{s}) = G_{E\delta}\delta(\mathbf{s}). \tag{4.8}$$

The function $g(E)$ which defines the energy dependence of the nucleus-nucleus potential in Eqs. (4.3) and (4.4) reads [69]: $g(E) = 1 - k_v E$, where E is the energy per nucleon. The values of all the coefficients, namely $r_i, G_{Di}, G_{Ei}, G_{E\delta}$ and k_v, are collected in Table 4.2. The choice of all coefficients above is beyond the scope of this work; we simply follow the prescriptions available in the literature.

It is widely known that the original density-independent M3Y interaction failed to saturate cold nuclear matter. In order to obtain the correct value of the central nucleon density and nucleon binding energy several versions of a density-dependent M3Y interaction have been proposed (see e.g., Ref. [71]). A generalized density dependence of the M3Y interaction was introduced in Ref. [71]. It enters as a multiplier $F(\rho_{DA}, E)$ for the density-independent NN interaction. The function F is given by

$$F(\rho_{DA}, E) = C_{\rho_{DA}}\{1 + \alpha(E)\, exp(-\beta(E)\rho_{DA}) - \gamma(E)\rho_{DA}\}\,. \tag{4.9}$$

The choice of the nucleon density ρ_{DA} is specified below. If the M3Y-Paris NN interaction is used, this density dependence results in the correct saturation binding energy of about 16 MeV/nucleon and a nuclear density of 0.17 fm^{-3}, for several sets of coefficient that are presented in Table 4.3. The different parameter sets in Table 4.3 result in different values of nuclear matter incompressibility, ranging from 176 MeV for the

Table 4.2: The coefficients of the Reid and Paris M3Y interactions.

Coefficient	Reid	Paris
G_{D1} (MeV)	7999	11062
G_{D2} (MeV)	-2134	-2537.5
G_{D3} (MeV)	0	0
G_{E1} (MeV)	4631.4	-1524.25
G_{E2} (MeV)	-1787.1	-518.75
G_{E3} (MeV)	-7.847	-7.847
r_1 (fm)	0.25	0.25
r_2 (fm)	0.40	0.40
r_3 (fm)	1.414	1.414
$G_{E\delta}$ (MeV fm^3)	-276	-592
k_v (MeV^{-1})	0.002	0.003

DDM3Y1 interaction up to 270 MeV for the BDM3Y1 interaction. The original density-independent M3Y NN forces correspond to parameter set DD0 in this table. The use of density-dependent forces means that the bare M3Y direct and exchange NN interactions, $v_D(s)$ and $v_E(s)$, in Eqs. (4.3) and (4.4) should be replaced by

$$\varphi_{D(E)}(s, \rho_{DA}) = F(\rho_{DA}, E) v_{D(E)}(s)\,. \tag{4.10}$$

The nucleon density ρ_{DA} appearing in Eqs. (4.9) and (4.10) has to be specified before any calculations of the double folding potential can be performed. In Eq. (4.9) for the direct forces, ρ_{DA} is taken to be equal to $\rho_{1A}(\mathrm{r}_1) + \rho_{2A}(\mathrm{r}_2)$ [67]. While in Eqs. (4.10), describing the exchange forces, $\rho_{DA} = \rho_{1A}(\mathbf{r}_1 + \mathbf{s}/2) + \rho_{2A}(\mathbf{r}_2 - \mathbf{s}/2)$ [69, 71]. This corresponds to the density at the midpoint between two interacting nucleons and is found to have some physical justification.

Table 4.3: The coefficients of the generalized density-dependent M3Y NN interactions of Eq. (4.9), compiled from Ref. [71].

DD label	Interaction	C	α	$\beta(\text{fm})^{-3}$	$\gamma(\text{fm})^{-3}$
0	D independent	1	0.0	0.0	0.0
1	DDM3Y1	0.2963	3.7231	3.7384	0.0
2	CDM3Y1	0.3429	3.0232	3.5512	0.5
3	CDM3Y2	0.3346	3.0357	3.0685	1.0
4	CDM3Y3	0.2985	3.4528	2.6388	1.5
5	CDM3Y4	0.3052	3.2998	2.3180	2.0
6	CDM3Y5	0.2728	3.7367	1.8294	3.0
7	CDM3Y6	0.2658	3.8033	1.4099	4.0
8	BDM3Y1	1.251	0.0	0.0	1.7452

4.1.2 Density Dependent and α-nucleus Potential

Although, the above description for generalized DFM had an undisputed success for heavy ions reactions with the parameters given in Tables 4.2 and 4.3, we use in our study the work of Chaudhuri [72], which is well suited for α-nucleus interactions as it accounts for the higher order exchange effects and the Pauli blocking correctly. In that work the M3Y-Reid effective nucleon-nucleon interaction supplemented by a density-dependent term was used. The resultant model (called DDM3Y) gave a consistent picture of elastic scattering.

For the density-independent part, the direct term of Eq. (4.3) and the delta simulated form of the exchange term Eq. (4.8) were used. This is known as a zero-range pseudopotential [68]. Equation (4.8) then becomes

$$v_{E\delta}(s) = J_{00}(E)\delta(s)\,, \tag{4.11}$$

with

$$J_{00}(E) = -276\left(1 - 0.005\frac{E}{A_\alpha}\right)\,(\mathrm{MeV\,fm^3})\,. \tag{4.12}$$

In the case of the density-dependent part, Eq. (4.9) was factorized into a product function consisting of the density functions of the target and projectile term [see [72]], i.e.

$$t(\rho_1, \rho_2, E) \equiv F(\rho_{DA}, E) = Cf(\rho_1, E)f(\rho_2, E)\,, \tag{4.13}$$

and the function $f(\rho_i, E), i = 1, 2$ is given by

$$f(\rho_i, E) = 1 - \beta(E)\rho_i^{2/3} \qquad\qquad i = 1, 2\,. \tag{4.14}$$

This assumption is based on the insensitivity of the density parameters to the nature of the projectile.

In the energy regime 100 MeV to 172 MeV, the typical potential depth of α-decay, by fitting elastic alpha scattering data, the strength parameter $C = 1.3$ and the density parameter $\beta = 1.01$ were obtained. It should, however, be noted that other values of C and β are possible.

4.1.3 Charge and Nucleon Density Distributions

Finally, the densities appearing in Eq. (4.3) and (4.4) are *matter* densities (sometimes called "point densities"). However, densities derived from electron scattering are *charge* densities and must be corrected for the nucleon charge distribution before they are used. This is conveniently done in momentum space as suggested and implemented by Cook [73]. For simplicity, if it is assumed that the neutron density ρ_n is proportional to the proton density ρ_p: $\rho_\mathrm{n} = (N/Z)\rho_\mathrm{p}$ as is often done for nuclei with $N \approx Z$; then the radii of the proton and charge distributions are related by [68]

$$\langle r^2\rangle_\mathrm{p} \approx \langle r^2\rangle_\mathrm{ch} - 0.76 + 0.11(N/Z)\,. \tag{4.15}$$

To keep our calculations simple and numerically convenient, we have used model densities given by [59, 65, 72]. Thus for the α-particle a Gaussian parametrization given by

$$\rho_1(r) = 0.4229 \exp(-0.7024 r^2)\,, \tag{4.16}$$

whose volume integral is equal to A_α $(= 4)$ is used. The density distribution function ρ_2 used for the targets (i.e. the daughter nuclei) is chosen to be of the spherically symmetric Woods-Saxon form given by

$$\rho_2(r) = \frac{\rho_0}{1 + \exp((r-c)/a)}\,, \tag{4.17}$$

where

$$c = r_\rho(1 - \pi^2 a^2/3r_\rho^2), \quad r_\rho = 1.13 A_d^{1/3} \quad \text{and} \quad a = 0.54\,\text{fm}\,, \tag{4.18}$$

and the value of ρ_0 is fixed by equating the volume integral of the density distribution function to the mass number A_d of the residual daughter nucleus.

4.2 Decay Widths

4.2.1 Method A: Quasi-bound state wavefunction approach

In the usual microscopic approach, the calculation of the decay width [Eq.(3.18)] requires knowledge of the (quasistationary) initial state wave function of the parent nucleus, the final state wave functions of the product nuclei, and the interaction potential.

This isolated quasistationary state Φ is obtained by integrating the radial Schrödinger equation given by equation (3.15) numerically. If Coulomb forces are included, the solution to the Schrödinger equation (for large r) is a linear combination of the regular and irregular Coulomb functions which look like, respectively,

$$F(z) \sim \sin\left(z - \eta\, \ln\, 2z - \ell\frac{\pi}{2} + \sigma_\ell\right)$$

and

$$G(z) \sim \cos\left(z - \eta \ln 2z - \ell\frac{\pi}{2} + \sigma_\ell\right) . \tag{4.19}$$

Here σ_ℓ stands for the usual Coulomb phase shift and η for the Sommerfeld parameter. Clearly, the quasibound resonant state wavefunction behaves like $G(r)$ asymptotically, which is one of the boundary conditions. The other boundary conditions employed are:

- $r\Phi \to 0$ as $r \to 0$, and
- Φ shall have a specified number of internal nodes.

It is not possible to satisfy all these conditions with any arbitrary nuclear potential $V(r)$. The parameters of the potential must be varied. One determines a normalized resonant state in the internal region of the one-body potential $V(r)$ (see e.g. Eq. (3.40)) until the external turning point by using the standard matching procedure as described in section 3.2.1. In this work, the nuclear potential $V(r)$ is given as a simple nuclear optical potential of a Woods-Saxon type. Since in α-decay there is no absorption, we completely ignore the imaginary part of the optical potential making the nuclear potential real. For fixed Woods-Saxon radius and diffuseness, and for energy $E(= Q)$ and quantum numbers $n\ell j$ of the quasibound state, the depth of the nuclear potential is iteratively adjusted until the inner and outer wave functions are smoothly connected.

In this method, we solve equations (3.15), (3.16) and (3.17) for the outgoing Coulomb amplitude C_ℓ. The radial wave function of the α-particle in the quasibound state is given by

$$\Phi_{n\ell j}(r) = \frac{\phi_{n\ell j}(r)}{r} . \tag{4.20}$$

The quasibound α-particle wave function $\phi_{n\ell j}(r)$ is found by joining smoothly the wave function from the interior region with the outgoing Coulomb wave function at large distance.

To determine the amplitude multiplying the outgoing Coulomb wave, instead of matching the outgoing Coulomb wave function with the α-cluster formation amplitude as is normally done in standard microscopic approach (see Eq. (3.17)), we replace the right-hand side of equation (3.17) with the internal resonant wave function obtained by solving equation (3.15) i.e.

$$\phi_{n\ell j}(R) = C_\ell[G_\ell(kR) + iF_\ell(kR)], \tag{4.21}$$

using equation (4.20) in equation (4.21) and solving for C_ℓ we obtain

$$C_\ell = \frac{R\Phi_{n\ell j}(R)}{G_\ell(kR) + iF_\ell(kR)}$$

therefore

$$|C_\ell|^2 = \frac{R^2\Phi^2_{n\ell j}(R)}{G^2_\ell(kR) + F^2_\ell(kR)}\,. \tag{4.22}$$

The decay width is now obtained from equation (3.19) by substituting equation (4.22) i.e.

$$\Gamma_\ell = \hbar v\,\frac{R^2\Phi^2_{n\ell j}(R)}{G^2_\ell(kR) + F^2_\ell(kR)}\,. \tag{4.23}$$

Since $F_\ell(kr) \ll F_\ell(kr)$ inside the barrier, further approximation is justified, namely,

$$\Gamma_\ell = \hbar v\,\left[\frac{R\Phi_{n\ell j}(R)}{G_\ell(kR)}\right]^2 \tag{4.24}$$

The model parameters employed are specified and discussed in section 4.3.

4.2.2 Method B: SAFM and DFM

The half-lives of the parent nuclei within the framework of the SAFM as described in section 3.2.3 requires the evaluation of the microscopic nuclear interactions of the α-particle and daughter nuclei using the DFM formalism.

The total interaction potential used in this method is given by equation (3.40). In section 3.2.3, a detailed description of the method and formulae needed within this

framework have been presented.

Below we summarized the DFM formulae and data appropriate for our work. The M3Y effective interaction with the Reid parameters we used in this dissertation is very popular. They are:

$$\begin{aligned} U_N(R) &= \lambda_0 \iint \rho_1(\vec{r_1})\rho_2(\vec{r_2}) v[|\vec{r_2} - \vec{r_1} + \vec{R}| \equiv s]\, d^3r_1\, d^3r_2\,, \\ v(s,\rho_1,\rho_2,E) &= u^{M3Y}(s,E)\, t(\rho_1,\rho_2,E)\,, \\ u^{M3Y}(s,E) &= A\frac{e^{-\beta_1 s}}{\beta_1 s} + B\frac{e^{-\beta_2 s}}{\beta_2 s} + J_{00}(E)\delta(s)\,, \\ t(\rho_1,\rho_2,E) &= C(1-\beta(E)\rho_i^{2/3})(1-\beta(E)\rho_i^{2/3})\,, \end{aligned} \tag{4.25}$$

with λ_0 of order unity and

$A = G_{D1}, \qquad B = G_{D2}, \qquad J_{00} = G_{E\delta}, \qquad \beta_1 = 1/r_{v1}, \qquad \beta_2 = 1/r_{v2}$

$C = 1.0, \qquad \beta(E) = 1.6.$

Other values of C and $\beta(E)$ are possible. For optimum fit to experimental data, these values of C and $\beta(E)$ must be chosen carefully (see section 5.2.1).

In the present calculation, the double folding potential is calculated using the computer code DFPOT [73].

A typical situation of the total interaction (sum of nuclear, coulomb and centrifugal potentials) used in this work is shown in Fig. 4.2

4.2.3 Method C: QCA and DFM

For low-lying metastable states, the quasiclassical method (WKB) is expected to work very well. The quasiclassical expressions for Γ can be derived from the two-potential approach [15]. In particular, the decay width is given in equation (3.8). For the nuclear interaction, we use the same DFM potential summarized in Method B (see Eq. (4.25)), which is different from the usual PCM method. The Coulomb potential is taken in the usual form of either PCD or SCD where the Coulomb radius R_C has been chosen identically with the *rms* radius of the folding potential $V_N(r)$.

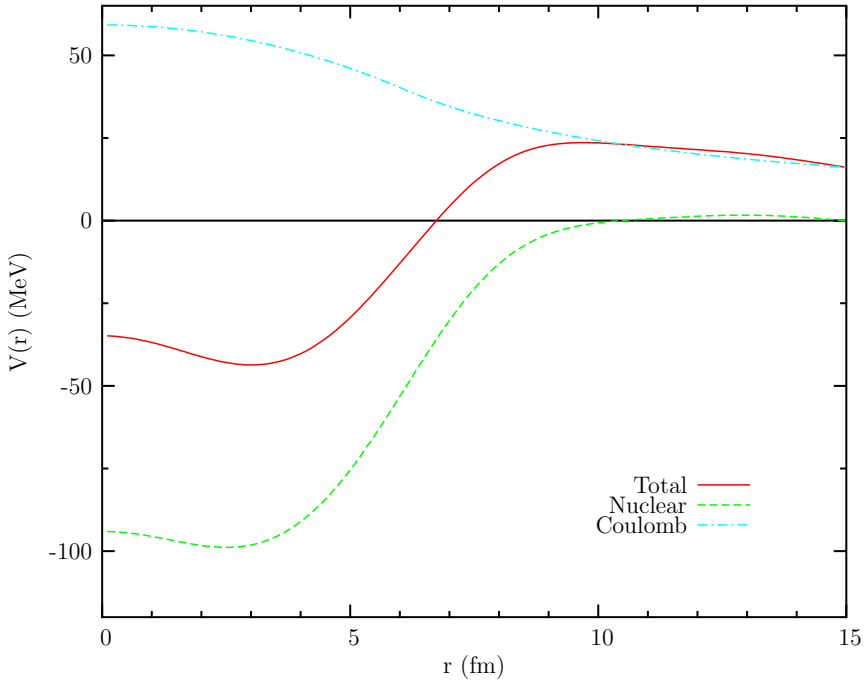

Figure 4.2: A typical DF potential for the system ^{216}Rn $\rightarrow$ ^{208}Po + α. The nuclear DFM potential V_N, the Coulomb V_C and the total interaction V are shown.

In this work, we calculate the α-decay widths and half-lives of different α emitters using equations (3.8), (3.10), (3.11) and (3.12). The Q-value and the preformation factor, which are of optimum importance in this analysis, are not taken in the usual manner of the PCM. It must be pointed out that the preformation factor should be smaller than unity because the simple two-body model assumes that the ground state wave function of the α emitter contains a pure α-daughter configuration [23]. The decay width in this model therefore always overestimates the experimental decay width. Consequently, we determine the preformation factor P from the ratio between the calculated and the measured half-lives [56].

4.3 Model parameters

The systems we consider in this work are chosen based on availability of the experimental ground state masses for the parent and daughter nuclei. This set was selected because there is no uncertainty in the determination of the released energy Q which is one of the crucial quantities for the quantitative prediction of decay half-lives. In all the Methods, the Q-value of the system is determined using Eq. (2.4), the masses are taken from the mass excess table of Audi and Wapstra [75].

In Method A, the α optical potential V_N was approximated by an average Woods-Saxon (WS) field, containing only a central term. The WS form factor is defined by the radius, $R_0 = r_0 A^{1/3}$, and diffuseness a. It is well known that considerable ambiguities exist in the values of the parameters for the α-nucleus optical potentials. Several potentials, which give the same phase shifts, will also give the same scattering cross section.
Two separate sets A and B of WS parameters [45, 76] have been considered. The sets were obtained after detailed analyses of the scattering of α-particle and rigorous study of these ambiguities. Since the imaginary parts are not needed for our present purpose, only the real parameter values of the two sets are listed in Table 4.4. The depth of the potential, V_0, has not been taken from Refs. [45, 76], but rather adjusted to reproduce the experimental energy of a quasistationary state with a specified number of nodes.
The Coulomb potential equation (3.5) is used. The Coulomb radius R_C is given by $r_c A^{1/3}$, the radius parameter r_c is also shown in Table 4.4.
The parameters adopted for both Methods B and C have already been explained and explicitly discussed in section 4.2.2.

Table 4.4: Woods-Saxon parameters (r_0 and a) of α-nucleus potential used in the calculation. Coulomb radius is r_c.

Parameter	Set A	Set B
r_0 (fm)	1.342	1.454
a (fm)	0.566	0.560
r_c (fm)	1.3	1.3

Chapter 5

Results: Analysis and Discussion

The effectiveness of an alpha decay theory depends on how well it can reproduce or predict the decay rates with the least number of adjustable parameters, when Q-value and the orbital quantum number ℓ are known.
The results presented here are based on the three different models of Chapter 4 applied in calculating the decay widths and half-lives of α-nucleus systems.

As already mentioned, our choice of the models is purely based on numerical computation, conveniency and least number of adjustable parameters.

5.1 Method A: Numerical results

We first perform calculation based on Method A. The α-nucleus optical potentials for two of the systems considered: ^{212}Po and ^{144}Nd are shown in Fig. 5.1 using the parameters of Set A.

The calculated wave function $\Phi_{n\ell j}(r)$ of the systems are shown in Fig. 5.2 and Fig. 5.3. As expected, in the interior region ($r \lesssim 10$) fm the wave functions have 11 and 10

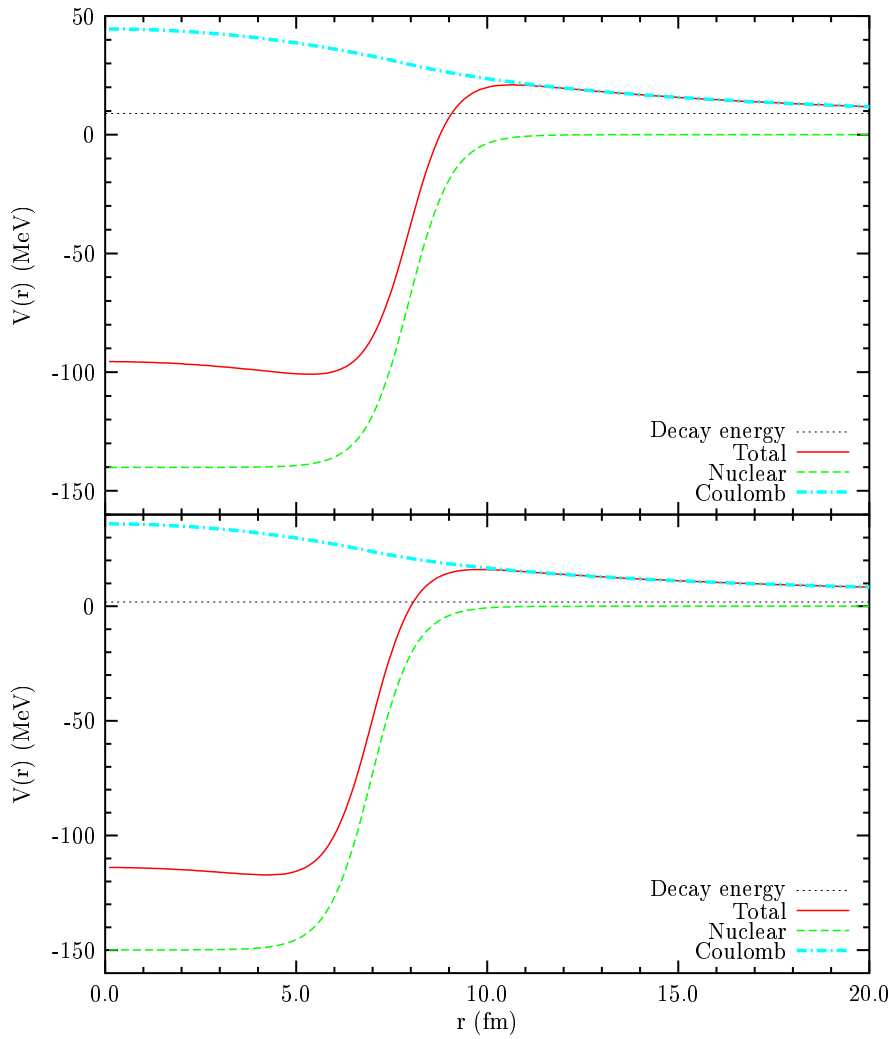

Figure 5.1: The upper and lower figure show the optical potential V_N and the Coulomb interaction V_C for the nuclei ^{212}Po and ^{144}Nd, respectively. The Q-values are also included.

nodes, respectively. The outer turning point is at about 27 fm and 87 fm for Po and Nd, respectively. This results in a reduction of the wave function in the barrier region by about 7 orders of magnitude for ^{212}Po and about 18 orders of magnitude for ^{144}Nd. In the outer region, outside the classical outer turning point, the characteristic oscillatory behaviour of the Coulomb function is seen in both cases.

Figures 5.4 and 5.5 illustrate the radial dependence of the three terms involved in calculating the decay width of equation (4.23): the normalized quasibound wave function,

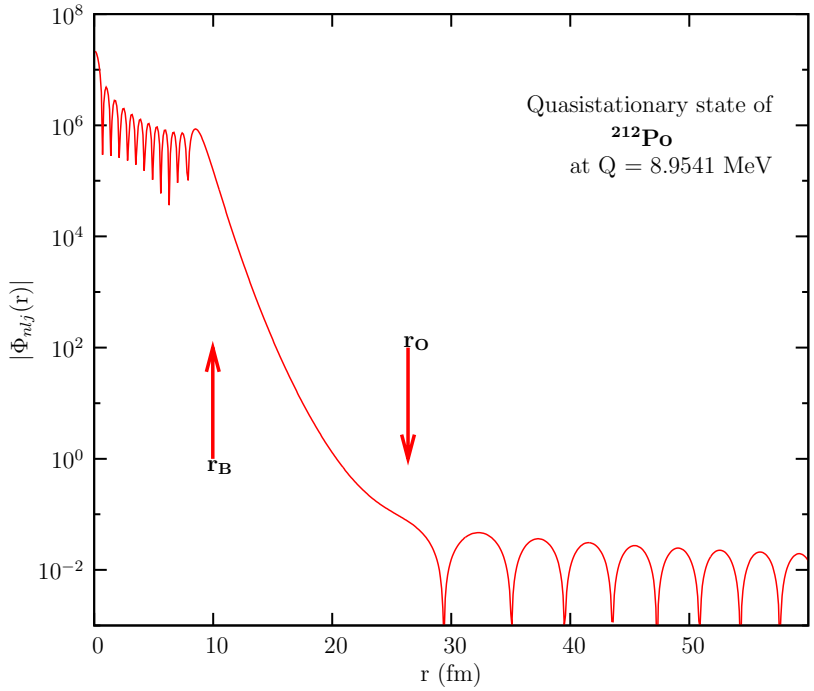

Figure 5.2: Spherical radial wave function of the quasistationary state at 8.9541 MeV in ^{212}Po (in logarithmic scale) as a function of r. The Coulomb barrier radius, $r_B = 10.4$ fm, and the outer classical turning point $r_O = 26.3$ fm, are indicated.

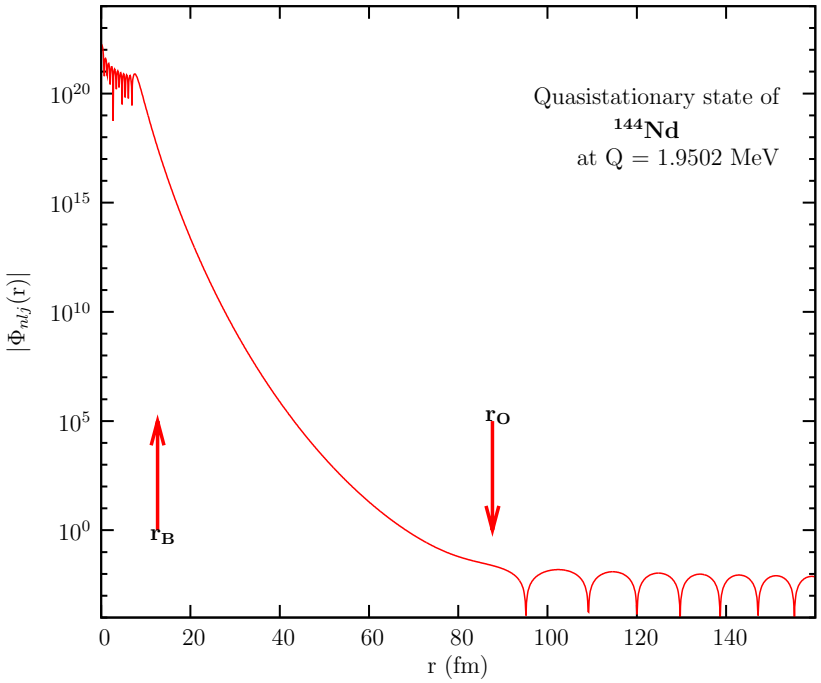

Figure 5.3: Same as in Fig. 5.2 but for ^{144}Nd.

$\Phi_{n\ell j}(r)$, the regular and irregular Coulomb function, $F_\ell(r)$ and $G_\ell(r)$. The dependence of the Coulomb penetration factor P_ℓ on the radius is illustrated on Fig. 5.6 alongside the one-body reduced width γ_ℓ. The tremendous dependence of γ_ℓ on r is somewhat compensated by the corresponding dependence of P_ℓ on r. The main contribution to

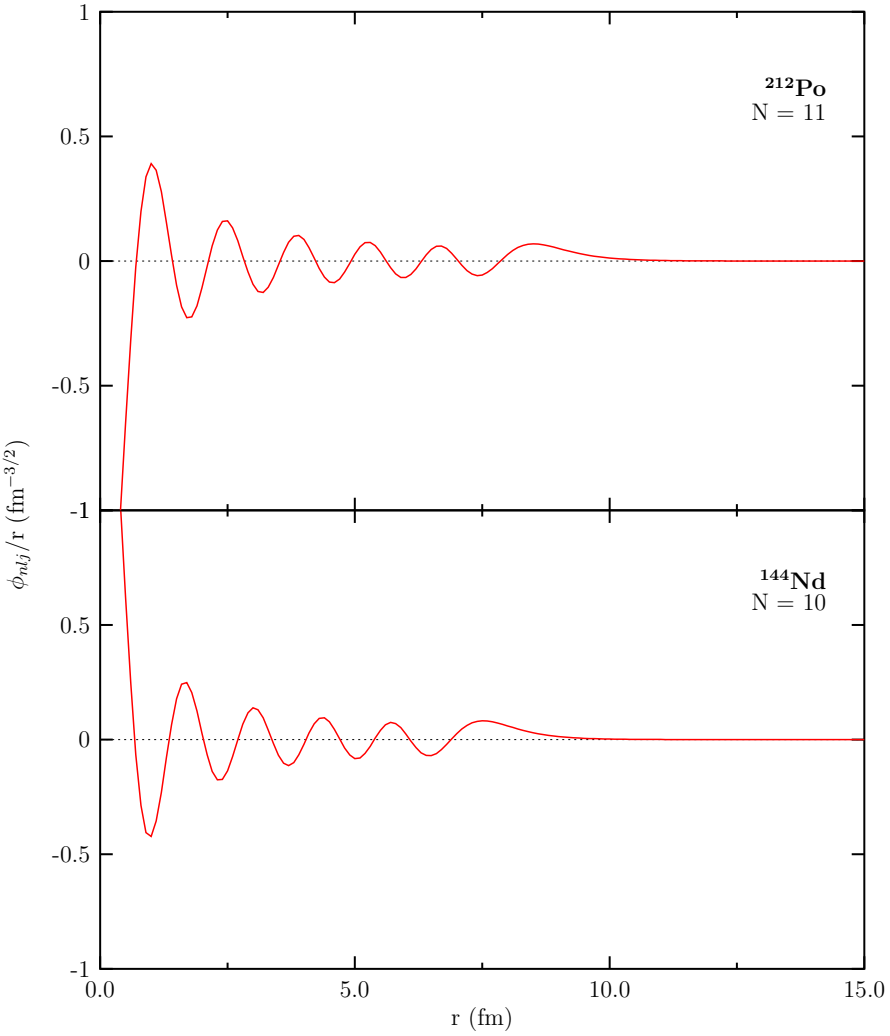

Figure 5.4: The normalized quasibound radial wave function $\Phi_{n\ell j}(r)$ for ^{212}Po and ^{144}Nd as a function of r. The number of nodes N for each nuclei, are indicated.

the decay width is seen to come from the surface region, where P_ℓ and the reduced width γ intersect and their product is maximum. This is seen to occur around the nuclear surface R_i (see below). This is because the Coulomb function is vanishingly small at small

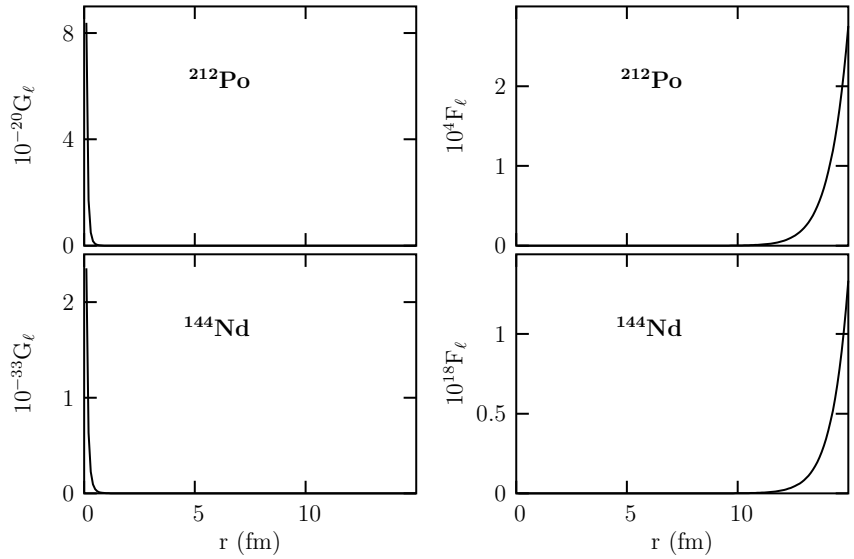

Figure 5.5: The Coulomb wave functions: regular $F_\ell(r)$ and irregular $G_\ell(r)$ for ^{212}Po and ^{144}Nd as a function of r. F_ℓ is vanishingly small at small r while the usual high values for G_ℓ is seen.

r values, while the wave function of the quasistationary state decreases exponentially in the barrier region (cf. Fig. 5.2). The α-decay rate is thus expected to depend rather weakly on the detailed structure of the wave function in the interior part of the nucleus, while surface properties may be important.

The depths of the optical potential obtained after adjusting to the energy of the α-particle and the specified number of nodes are shown in Table 5.1. As seen in Table 5.1, the outer classical turning points R_o are identical for the systems due to the fact only Coulomb interaction remains for large radial distances. The inner turning point R_i depends strongly on the potential depths and the number of nodes as is seen in Table 5.1, it is therefore very important that the matching point of the resonant wave function in the internal and outer regions be chosen carefully. In this work, we match the wave function at the inner turning point, which is presumably near the touching configuration as explained in section 3.2.1. It is reasonable to suppose that alpha formation more readily occurs in the surface region than in the nuclear interior. This reason is exemplified in Fig. 5.6.

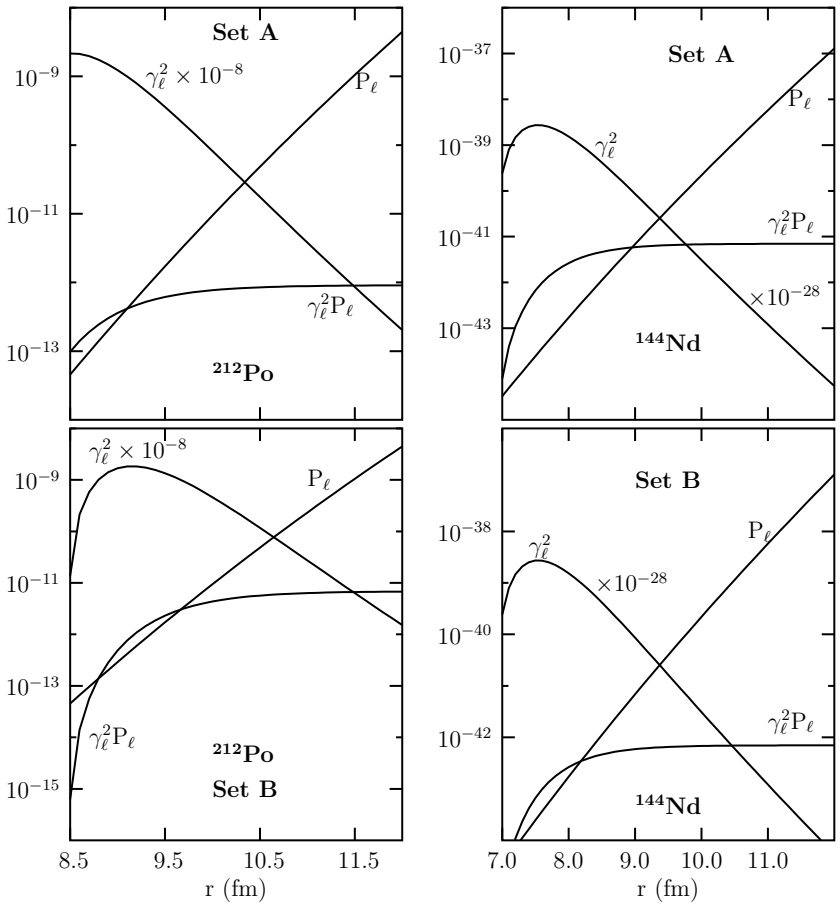

Figure 5.6: Coulomb penetration factor $P_\ell(r)$, formation probability γ_ℓ^2 and their product $\gamma_\ell^2 P_\ell$ for the transitions ^{144}Nd $\rightarrow$ ^{140}Ce + α and ^{212}Po $\rightarrow$ ^{208}Pb + α for the two sets of parameters A and B.

The half-lives of our systems calculated within the framework of Method A are given in Table 5.2. Comparison between the calculated and measured decay widths for the two sets are presented in Table 5.3. If one is satisfied with the order-of-magnitude estimate, the paramater Set A is found to be superior to Set B. In all the 16 decays examined the calculations reproduced the half-lives to within a factor 27 or better with the exception of the nuclei ^{208}Po and ^{217}Th. The reason for this exception is due to the effects of proton and neutron shell closures on α-decay half-lives [11]. Also, for the case of ^{217}Th, the effect of angular momentum on the outside solution is such as to decrease Γ, since $\ell(\ell+1)/r^2$ is considered as an addition to the barrier, making it higher and thicker.

Table 5.1: Comparison of the optical potential depths, the inner and outer classical turning points of the two parameter sets A and B of Table 4.4.

Nucleus	Node	Set A			Set B		
	N	V_0	R_i	R_o	V_0	R_i	R_o
^{144}Nd	10	150.57	8.071	87.666	132.91	8.606	87.666
^{146}Sm	10	149.84	8.100	68.324	132.28	8.640	68.324
^{150}Gd	11	148.41	8.149	63.564	131.08	8.695	63.564
^{152}Gd	11	148.09	8.160	80.987	130.87	8.708	80.987
^{174}Hf	11	160.60	8.500	80.801	141.86	9.076	80.801
^{190}Pt	11	155.10	8.680	67.352	137.18	9.279	67.352
^{208}Po	12	147.90	8.909	45.276	130.86	9.533	45.276
^{212}Pb	12	140.99	9.073	26.372	124.32	9.712	26.372
^{216}Rn	12	159.68	9.163	29.499	140.60	9.800	29.499
^{224}Ra	12	160.77	9.167	42.781	141.94	9.808	42.781
^{232}Th	12	160.92	9.199	62.070	142.36	9.845	62.070
^{240}Cm	12	158.03	9.304	42.314	139.78	9.963	42.314
^{256}Fm	12	153.43	9.465	40.162	135.81	10.142	40.162
^{217}Th	12	151.22	9.136	27.008	133.12	9.779	27.008
^{227}Ac	12	143.51	9.090	49.688	127.22	9.735	49.688
^{229}U	12	142.60	9.128	40.026	126.36	9.778	40.026

The effect of this nonzero ℓ on the interior solution is determined through the increment of the wave number with ℓ. This increase indicates a greater kinetic energy inside the nucleus and hence more frequent collisions with the surface. This situation is reflected in the reduced value of the one-body reduced width (cf. Fig. 5.6).

Unfortunately, none of the paramater sets give completely satisfactory results. In order to find useful parameters for V_N, we have to make a more systematic parameter search,

Table 5.2: Alpha decay half-lives calculated within Method A.

Parent			Set A	Set B	
Z	A	Q (MeV)	$T_{1/2}^{calc}$ (s)	$T_{1/2}^{calc}$ (s)	$T_{1/2}^{expt}$ (s)
60.	144.	1.9052	1.541×10^{22}	2.429×10^{21}	7.219×10^{22}
62.	146.	2.5289	3.495×10^{14}	5.427×10^{13}	3.248×10^{15}
64.	150.	2.8089	6.603×10^{12}	9.860×10^{11}	5.646×10^{13}
64.	152.	2.2046	5.545×10^{20}	7.971×10^{19}	3.406×10^{21}
72.	174.	2.4948	6.347×10^{22}	7.534×10^{21}	6.307×10^{22}
78.	190.	3.2495	5.025×10^{17}	5.272×10^{16}	2.050×10^{19}
84.	208.	5.2155	7.056×10^{5}	7.002×10^{4}	9.139×10^{7}
84.	212.	8.9541	1.138×10^{-8}	1.409×10^{-9}	2.990×10^{-7}
86.	216.	8.2001	3.461×10^{-6}	3.968×10^{-7}	4.500×10^{-5}
88.	224.	5.7889	2.538×10^{4}	2.370×10^{3}	3.162×10^{5}
90.	232.	4.0827	6.557×10^{16}	5.236×10^{15}	4.431×10^{17}
96.	240.	6.3972	1.094×10^{5}	8.720×10^{3}	2.345×10^{6}
100.	256.	7.0269	5.687×10^{3}	4.210×10^{2}	1.167×10^{5}
90.	217.	9.4240	3.027×10^{-3}	6.697×10^{-2}	2.520×10^{-4}
89.	227.	5.0422	1.878×10^{9}	1.597×10^{8}	4.975×10^{10}
92.	229.	6.4752	1.437×10^{3}	1.245×10^{2}	1.740×10^{4}

taking configuration mixing into account. However, it should be noted that both potential sets give the same penetrability but they give different values for the α width. Variation of the optical model parameters within their uncertainties affects the predicted half-lives by not much than a factor of 7 to 9. The sensitivity of $T_{1/2}$ to the details of the optical α potential has been known for very long time [45]. It is well known that more than 85–94 % of the penetrability, P_ℓ, comes from the region $r > r_B$, the Coulomb barrier radius, which is almost solely determined by the combined Coulomb + centrifu-

Table 5.3: Alpha decay widths calculated in the QSWA method with the two parameter Set A (Γ_A) and Set B (Γ_B), compared with the experimental data (Γ_{exp})

Parent		Set A	Set B	Expt.		
Z	A	Γ_A (MeV)	Γ_B (MeV)	Γ_{exp} (MeV)	Γ_A/Γ_{exp}	Γ_B/Γ_{exp}
60.	144.	2.960×10^{-44}	1.878×10^{-43}	6.320×10^{-45}	4.68	29.72
62.	146.	1.305×10^{-36}	8.407×10^{-36}	1.405×10^{-37}	9.29	59.85
64.	150.	6.910×10^{-35}	4.627×10^{-34}	8.082×10^{-36}	8.55	57.25
64.	152.	8.227×10^{-43}	5.723×10^{-42}	1.340×10^{-43}	6.14	42.72
72.	174.	7.188×10^{-45}	6.056×10^{-44}	7.234×10^{-45}	0.99	8.37
78.	190.	9.080×10^{-40}	8.653×10^{-39}	2.226×10^{-41}	40.79	388.76
84.	208.	6.466×10^{-28}	6.516×10^{-27}	4.992×10^{-30}	129.52	1305.2
84.	212.	4.008×10^{-14}	3.239×10^{-13}	1.526×10^{-15}	26.27	212.29
86.	216.	1.318×10^{-16}	1.150×10^{-15}	1.014×10^{-17}	13.00	113.41
88.	224.	1.798×10^{-26}	1.925×10^{-25}	1.443×10^{-27}	12.46	133.41
90.	232.	6.958×10^{-39}	8.713×10^{-38}	1.030×10^{-39}	6.76	84.62
96.	240.	4.172×10^{-27}	5.232×10^{-26}	1.946×10^{-28}	21.44	268.89
100.	256.	8.023×10^{-26}	1.084×10^{-24}	3.908×10^{-27}	20.53	277.26
90.	217.	1.507×10^{-21}	6.812×10^{-21}	1.811×10^{-18}	0.008	0.038
89.	227.	2.429×10^{-31}	2.857×10^{-30}	9.171×10^{-33}	26.49	311.54
92.	229.	3.175×10^{-25}	3.664×10^{-24}	2.622×10^{-26}	12.11	137.93

gal interaction. Consequently, a rough estimate of $T_{1/2}$ can be obtained by ignoring the nuclear structure details.

5.2 Method B and C: Numerical results

The DFM potential plays a central role in Methods B and C. The results of Eq. (4.25) are used in determining the nuclear interaction.

5.2.1 Method B: SAFM and DFM

We next perform calculations based on the framework of the SAFM as described in section 3.2.3. We test this model using two different forms of the Coulomb interaction i.e. point (PCD) and spherical charge distributions (SCD). In addition, the effective interactions of M3Y and DDM3Y with zero-range psuedo-potential are used for the nuclear interaction.

The WKB action integral K (3.42) is determined by using simple Simpson' rule. After the integral has been evaluated, the half-lives of the α-decays is found by using equations (3.41) and (3.44). Following Basu's suggestion [77], the strength parameter C and the density-dependent parameter β appearing in equation (4.25) have been kept fixed at 1.0 and 1.6, respectively. This results from the optimum fit on the experimental data on α-decay. The zero-range pseudopotential $J_{00}(E)$ is also practically independent of energy for the decay process and has been taken as -276 MeV.fm^3.

The results of the calculations are summarized in Tables 5.4 and 5.5 for SCD and PCD, respectively. We plot the graphs of experimental data for logarithmic α-decay half-lives as a function of the mass numbers of the parent nuclei along with the results of the present calculations. Fig. 5.7 shows the distribution obtained using the SCD interactions. In the figure the open circles depict the experimental data while the continuous line with solid circles represents the corresponding calculations using the DDM3Y effective interaction and the dotted line represents calculations using the M3Y effective interaction supplemented by a zero-range pseudo-potential.

Table 5.4: Comparison between calculated α-decay half-lives using spherical charge distribution (SCD) for the Coulomb interaction and using effective interactions M3Y and DDM3Y with zero-range pseudo-potential for the nuclear interaction.

Parent			Theoretical value		Experimental value
			M3Y	DDM3Y	
Z	A	Q (MeV)	$T_{1/2}^{calc}$ (s)	$T_{1/2}^{calc}$ (s)	$T_{1/2}^{expt}$ (s)
60.	144.	1.9052	5.786×10^{21}	8.383×10^{21}	7.219×10^{22}
62.	146.	2.5289	2.372×10^{14}	3.619×10^{14}	3.248×10^{15}
64.	150.	2.8089	5.371×10^{12}	8.210×10^{12}	5.646×10^{13}
64.	152.	2.2046	2.701×10^{20}	3.946×10^{20}	3.406×10^{21}
72.	174.	2.4948	5.758×10^{22}	7.480×10^{22}	6.307×10^{22}
78.	190.	3.2495	9.028×10^{17}	1.095×10^{18}	2.050×10^{19}
84.	208.	5.2155	3.182×10^{6}	4.066×10^{6}	9.139×10^{7}
84.	212.	8.9541	6.200×10^{-8}	9.849×10^{-8}	2.990×10^{-7}
86.	216.	8.2001	3.011×10^{-5}	4.495×10^{-5}	4.500×10^{-5}
88.	224.	5.7889	2.225×10^{5}	2.638×10^{5}	3.162×10^{5}
90.	232.	4.0827	4.098×10^{17}	3.955×10^{17}	4.431×10^{17}
96.	240.	6.3972	1.602×10^{6}	1.575×10^{6}	2.345×10^{6}
100.	256.	7.0269	1.153×10^{5}	1.094×10^{5}	1.167×10^{5}
90.	217.	9.4240	1.695×10^{-5}	2.054×10^{-5}	2.520×10^{-4}
89.	227.	5.0422	1.949×10^{10}	2.102×10^{10}	4.975×10^{10}
92.	229.	6.4752	1.143×10^{4}	1.266×10^{4}	1.740×10^{4}

The results within the frame work of Method B is seen to predict the general trend of experimental data quite well. The quantitative agreement with experimental data is excellent. The reason for this, is partly, due to the that the effective nuclear potential is designed to properly describe decay properties and scattering wave functions. More

Table 5.5: The same as in Table 5.4 but using point charge distribution (PCD) for the Coulomb interaction.

Parent			Theoretical value		Experimental value
			M3Y	DDM3Y	
Z	A	Q (MeV)	$T_{1/2}^{calc}$ (s)	$T_{1/2}^{calc}$ (s)	$T_{1/2}^{expt}$ (s)
60.	144.	1.9052	5.786×10^{21}	8.821×10^{21}	7.219×10^{22}
62.	146.	2.5289	2.372×10^{14}	3.620×10^{14}	3.248×10^{15}
64.	150.	2.8089	5.373×10^{12}	8.216×10^{12}	5.646×10^{13}
64.	152.	2.2046	2.702×10^{20}	3.947×10^{20}	3.406×10^{21}
72.	174.	2.4948	5.993×10^{22}	7.509×10^{22}	6.307×10^{22}
78.	190.	3.2495	9.610×10^{17}	1.106×10^{18}	2.050×10^{19}
84.	208.	5.2155	3.397×10^{6}	4.129×10^{6}	9.139×10^{7}
84.	212.	8.9541	6.221×10^{-8}	9.888×10^{-8}	2.990×10^{-7}
86.	216.	8.2001	3.044×10^{-5}	4.537×10^{-5}	4.500×10^{-5}
88.	224.	5.7889	2.482×10^{5}	2.810×10^{5}	3.162×10^{5}
90.	232.	4.0827	4.965×10^{17}	4.282×10^{17}	4.431×10^{17}
96.	240.	6.3972	1.941×10^{6}	1.705×10^{6}	2.345×10^{6}
100.	256.	7.0269	1.429×10^{5}	1.190×10^{5}	1.167×10^{5}
90.	217.	9.4240	1.900×10^{-5}	2.108×10^{-5}	2.520×10^{-4}
89.	227.	5.0422	2.218×10^{10}	2.257×10^{10}	4.975×10^{10}
92.	229.	6.4752	1.295×10^{4}	1.355×10^{4}	1.740×10^{4}

importantly, the microscopic properties of the nucleons involved in the interactions (M3Y or DDM3Y) are taken into consideration with greater realibility.

The above results show that the differences in the α-decay lifetimes obtained using the spherical charge distributions or point charge distributions for calculating the Coulomb interaction are small. Introducing the density dependence and the zero-range pseudopo-

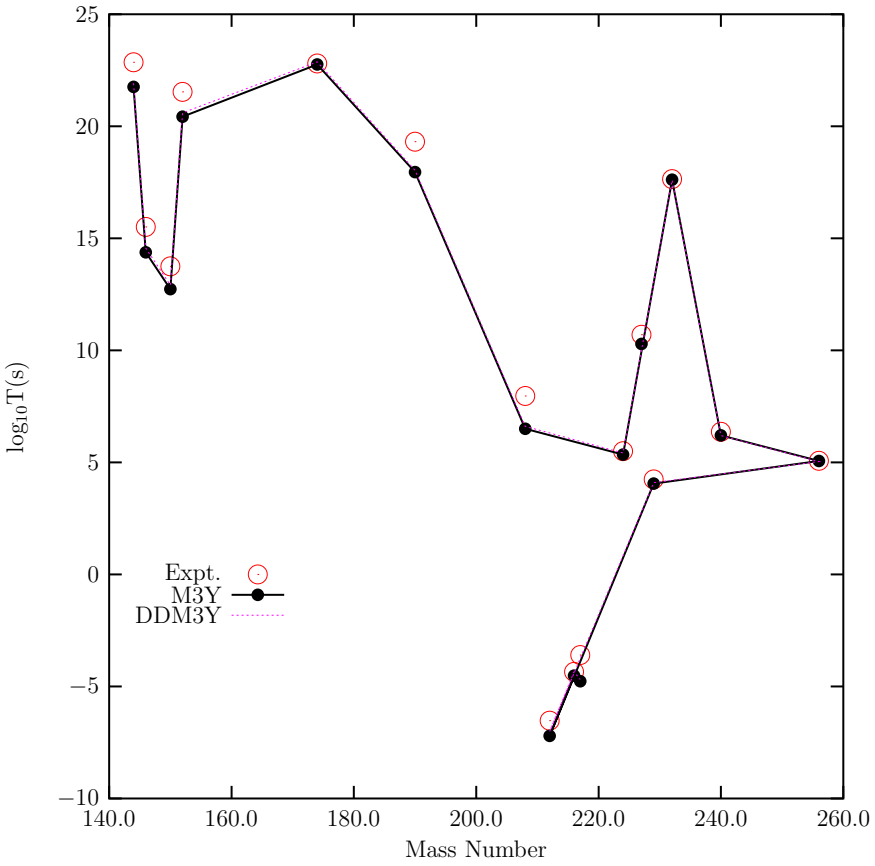

Figure 5.7: The logarithmic α-decay half-lives for the nuclei considered as a function of the parent mass number calculated in the M3Y and DDM3Y models. Experimental half-lives are indicated.

tential does not alter the general trend of the results. Use of the M3Y interaction alone for calculating the double folding nuclear interaction potentials is sufficient to provide reasonable estimates for the α-decay lifetimes.

In Table 5.6, the results of calculations of the turning points of the WKB action integral and SAFM calculations of the α-decay half-life from the nucleus ^{216}Rn have been presented which are obtained using the DDM3Y double folding potential with different normalization factor λ_0. The effect of the dependence of the inner turning point on λ_0 in calculating the half life is obvious from the table. This shows the effect the potential

depth has on decay lifetimes.

Table 5.6: Potential turning points and α-decay half life calculated using different normalization factor for DF potential with DDM3Y parametrization.

	Turning points			Theoretical
Normalization	First	Second	Decay width	half life
factor	(fm)	(fm)	$\Gamma(\mathrm{s}^{-1})$	$\log_{10} T(\mathrm{s})$
1.0	7.329	26.671	1.015×10^{-17}	-4.347
0.9	7.159	26.671	6.211×10^{-18}	-4.134
0.8	6.946	26.671	3.375×10^{-18}	-3.869
0.7	6.690	26.671	1.566×10^{-18}	-3.536
0.6	6.350	26.671	5.633×10^{-19}	-3.092
0.5	5.838	26.671	1.280×10^{-19}	-2.448
Experimental values:			1.014×10^{-17}	-4.347

5.2.2 Method C: PCM and DFM

We next present calculations within the model of section 4.2.3. In this method, the nuclear potential $V_N(r)$ is calculated within the DDM3Y parametrization and the SCD is used for the Coulomb interactions.

To calculate the decay widths for our systems, the classical turning points r_i appearing in equations (3.8) and (3.10) need to be determined. For $0^+ \rightarrow 0^+$ s-wave decay the innermost turning point is at $r_1 = 0$. r_2 varies from about 6 to 8 fm, and r_3 varies from 26 up to about 90 fm. In Table 5.7, we collected the values of these turning points used in our calculation. In addition, the *rms* values of the DF potential using the DDM3Y interactions are shown in the table as well. As remarked above, an effective potential is

Table 5.7: The values of the various radii needed for calculation of α-decay widths and half-lives for our systems in the framework of Method C. All parameters are in fm.

Parent		Turning points			
Z	A	r_1	r_2	r_3	r_{rms}
60.	144.	0.0	6.6272	87.6726	5.5663
62.	146.	0.0	6.6407	68.3289	5.5839
64.	150.	0.0	6.6604	63.5685	5.6186
64.	152.	0.0	6.6496	80.9930	5.6358
72.	174.	0.0	6.7479	80.8068	5.8169
78.	190.	0.0	6.8369	67.3567	5.9404
84.	208.	0.0	7.0163	45.2795	6.0723
84.	212.	0.0	7.3131	26.3738	6.1007
86.	216.	0.0	7.2516	29.5014	6.1288
88.	224.	0.0	7.1281	42.7845	6.1841
90.	232.	0.0	7.0554	62.0744	6.2382
96.	240.	0.0	7.1317	42.3173	6.2913
100.	256.	0.0	7.2332	40.1647	6.3943
90.	217.	1.8351	7.0240	27.5081	6.1358
89.	227.	0.0	7.0872	49.6915	6.2045
92.	229.	0.0	7.1227	40.0285	6.2181

presented which is designed to describe decay properties and scattering wave functions and which leads to realistic preformation factors P.

In the normal PCM (see section 3.1.2), a preformation factor $P = 1$ for even-even nuclei, as used in [13] seems to be the consequence of the specially shaped cosh potential of that work. As an example, we compare the potentials $V(r) = V_N(r) + V_C(r) + V_L(r)$ from this work and from [13] for the system ^{216}Rn $\rightarrow ^{212}$Po $+\alpha$ in Fig. 5.8. It is seen that the

rms radius of the potential from [13] is significantly smaller ($r_{rms} = 5.670\,\text{fm}$) than the *rms* radius of the folding potential ($r_{rms} = 6.129\,\text{fm}$). Therefore, the Coulomb barrier in [13] is significantly higher than in this work.

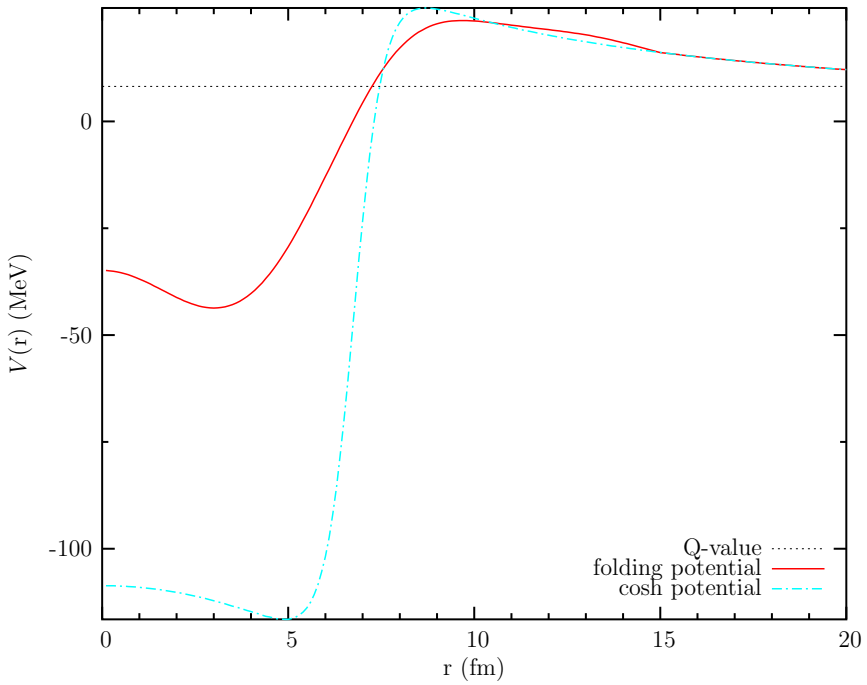

Figure 5.8: Comparison of the potential $V_N(r)$ from this work (folding potential, full line) and from [13] (cosh potential, dashed line) for the system $^{216}\text{Rn} \rightarrow {}^{208}\text{Po} + \alpha$. The deacy energy Q is indicated by a dotted line. Note the significantly higher Coulomb barrier in [13] compared to the folding potential.

The results of our calculation for the half-lives and decay widths for the data shown in Table 4.1 are summarized in Tables 5.8 and 5.9 respectively. As seen in Table 5.9, the calculated decay widths tend to over-estimate the measured decay widths. The reason for this is that we completely neglect the pure α-daughter configuration as pointed out above. This is motivated by the fact that the WKB exponent in equation (3.8) largely contribute to the value of the half-lives in the region of large r. In addition, the normalization constant $\lambda_0 = 1$ is used throughout in our calculation rather than

adjusting it to the bound state wave function with the specified number of nodes at the decay energy Q. Even in this first approximation, the decay widths calculated agree with the experimental data to a very good order.

Table 5.8: Alpha decay half-lives for the data in Table 4.1 using the Method C for our calculation.

Parent					
Z	A	Q (MeV)	$T_{1/2}^{calc}$ (s)	$T_{1/2}^{expt}$ (s)	P
60.	144.	1.9052	8.423×10^{22}	7.219×10^{22}	1.167
62.	146.	2.5289	2.768×10^{15}	3.248×10^{15}	0.852
64.	150.	2.8089	5.326×10^{13}	5.646×10^{13}	0.943
64.	152.	2.2046	4.065×10^{21}	3.406×10^{21}	1.194
72.	174.	2.4948	3.344×10^{23}	6.307×10^{22}	5.303
78.	190.	3.2495	2.146×10^{19}	2.050×10^{19}	1.047
84.	208.	5.2155	5.954×10^{7}	9.139×10^{7}	0.651
84.	212.	8.9541	2.895×10^{-7}	2.990×10^{-7}	0.968
86.	216.	8.2001	8.881×10^{-5}	4.450×10^{-5}	1.974
88.	224.	5.7889	9.468×10^{5}	3.162×10^{5}	2.994
90.	232.	4.0827	2.509×10^{18}	4.431×10^{17}	5.663
96.	240.	6.3972	7.733×10^{6}	2.345×10^{6}	3.298
100.	256.	7.0269	4.650×10^{5}	1.167×10^{5}	3.983
90.	217.	9.4240	1.429×10^{-4}	2.520×10^{-4}	0.567
89.	227.	5.0422	9.780×10^{10}	4.975×10^{10}	1.966
92.	229.	6.4752	4.979×10^{4}	1.740×10^{4}	2.862

In Fig. 5.9, we show the variation of the preformation factor with parent mass number. As expected, the value of P for ^{174}Hf in the neutron-deficient p nuclei region is unusually high. In the heavy nuclei region, the value of P is unnecessary high showing the effect

Table 5.9: Alpha decay widths for the data in Table 4.1 using the Method C for our calculation.

Parent					
Z	A	Q (MeV)	Γ_{calc} (MeV)	Γ_{expt} (MeV)	$\Gamma_{calc}/\Gamma_{expt}$
60.	144.	1.9052	5.4163×10^{-45}	6.3196×10^{-45}	0.857
62.	146.	2.5289	1.6480×10^{-37}	1.4047×10^{-37}	1.173
64.	150.	2.8089	8.5666×10^{-36}	8.0815×10^{-36}	1.060
64.	152.	2.2046	1.1222×10^{-43}	1.3397×10^{-43}	0.838
72.	174.	2.4948	1.3641×10^{-45}	7.2342×10^{-45}	0.189
78.	190.	3.2495	2.1261×10^{-41}	2.2258×10^{-41}	0.955
84.	208.	5.2155	7.6632×10^{-30}	4.9922×10^{-30}	1.535
84.	212.	8.9541	1.5758×10^{-15}	1.5258×10^{-15}	1.033
86.	216.	8.2001	5.1375×10^{-18}	1.0139×10^{-17}	0.507
88.	224.	5.7889	4.8187×10^{-28}	1.4428×10^{-27}	0.334
90.	232.	4.0827	1.8183×10^{-40}	1.0297×10^{-39}	0.177
96.	240.	6.3972	5.8999×10^{-29}	1.9458×10^{-28}	0.303
100.	256.	7.0269	9.8123×10^{-28}	3.9083×10^{-27}	0.251
90.	217.	9.4240	3.1922×10^{-18}	1.8105×10^{-18}	1.763
89.	227.	5.0422	4.6653×10^{-33}	9.1705×10^{-33}	0.509
92.	229.	6.4752	9.1639×10^{-27}	2.6224×10^{-26}	0.349

of not properly taking the bound state wavefunction into consideration.

5.3 Comparison of the Methods

The half-lives of the α emitters in Table 4.1 calculated with the different theoretical methods described in Chapter 4 are summarized in Table 5.10. In the table, we indicate

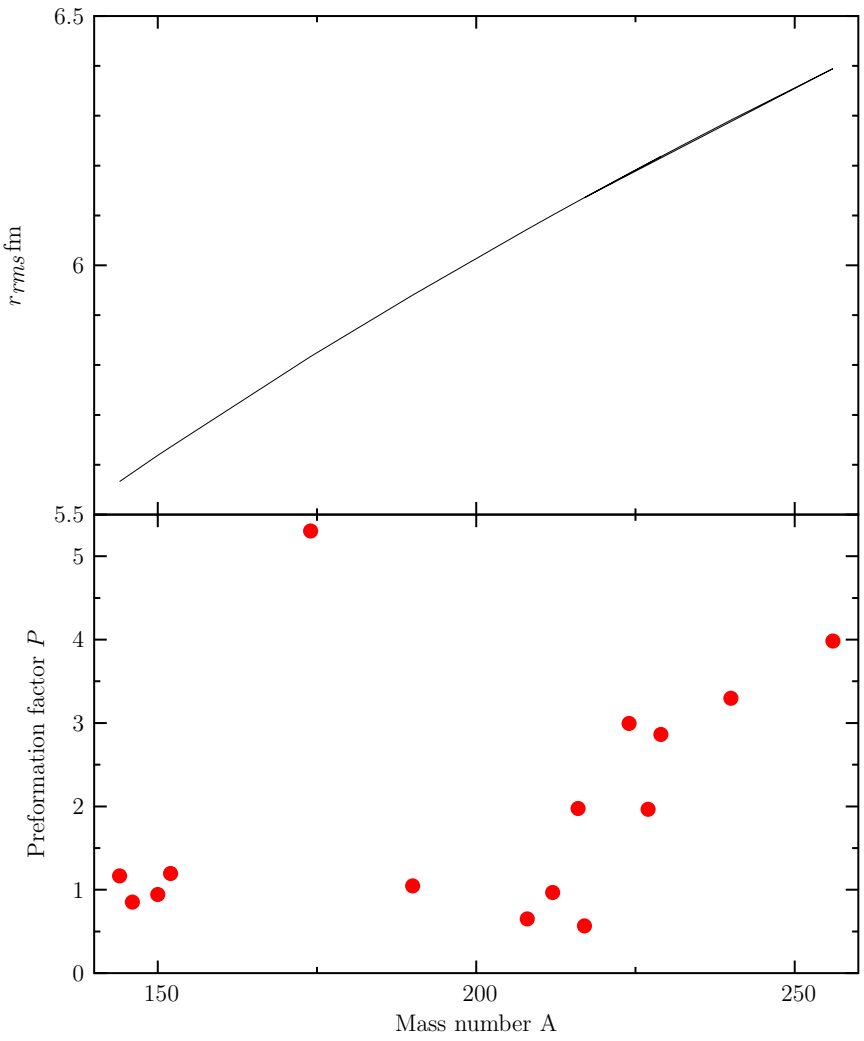

Figure 5.9: Variations of the preformation factor P and the root-mean-square values with the parent mass numbers for our data. The characteristic linear dependence of the *rms* value is seen from the figure.

only the results for Set A of QSWA and the DDM3Y with SCD interactions for Methods B and C.

As seen in Table 5.10, different methods applied in our work give similar results. If one is satisfied with the order-of-magnitude estimate, the simplest Method A is an excellent tool. The half-lives obtained with the Method A are within 10% of those with the Method B.

Table 5.10: Half-lives of α emitters $T_{1/2}^{calc}$ calculated with different methods. The Set A of the optical model parameters is used for Method A. DDM3Y with zero-range pseudopotential is used for the nuclear interactions for Methods B and C. The SCD interactions is assumed for Coulomb potential in all cases. The Q-values for the systems have been left out.

Nucleus	$T_{1/2}^{calc}$ (s)			$T_{1/2}^{expt}$ (s)
	A	B	C	
^{144}Nd	1.541×10^{22}	8.383×10^{21}	8.423×10^{22}	7.219×10^{22}
^{146}Sm	3.495×10^{14}	3.619×10^{14}	2.768×10^{15}	3.248×10^{15}
^{150}Gd	6.603×10^{12}	8.210×10^{12}	5.326×10^{13}	5.646×10^{13}
^{152}Gd	5.545×10^{20}	3.946×10^{20}	4.065×10^{21}	3.406×10^{21}
^{174}Hf	6.347×10^{22}	7.480×10^{22}	3.344×10^{23}	6.307×10^{22}
^{190}Pt	5.025×10^{17}	1.095×10^{18}	2.146×10^{19}	2.050×10^{19}
^{208}Po	7.056×10^{5}	4.066×10^{6}	5.954×10^{7}	9.139×10^{7}
^{212}Pb	1.138×10^{-8}	9.849×10^{-8}	2.895×10^{-7}	2.990×10^{-7}
^{216}Rn	3.461×10^{-6}	4.495×10^{-5}	8.881×10^{-5}	4.500×10^{-5}
^{224}Ra	2.538×10^{4}	2.638×10^{5}	9.468×10^{5}	3.162×10^{5}
^{232}Th	6.557×10^{16}	3.955×10^{17}	2.509×10^{18}	4.431×10^{17}
^{240}Cm	1.094×10^{5}	1.575×10^{6}	7.733×10^{6}	2.345×10^{6}
^{256}Fm	5.687×10^{3}	1.094×10^{5}	4.650×10^{5}	1.167×10^{5}
^{217}Th	3.027×10^{-3}	2.054×10^{-5}	1.429×10^{-4}	2.520×10^{-4}
^{227}Ac	1.878×10^{9}	2.102×10^{10}	9.780×10^{10}	4.975×10^{10}
^{229}U	1.437×10^{3}	1.266×10^{4}	4.979×10^{4}	1.740×10^{4}

The Method C yields half-lives which are closer to those obtained with Method B than method A in several cases. This result demonstrates that our first-order approximation of ignoring the effect of the bound state wavefunction is justified.

As discussed in section 4.3, in the QSWA calculations, the depth of the central potential V_0, has been adjusted to reproduce the experimental Q-value. Formally, when making the

adjustment, one should correct for the energy shift between the "true" quasistationary state and the "bound state" energy. This correction might be important in some cases, since the value of V_0 appears in the reduced width (see Eq. (4.23)) and in the WKB exponent of Methods B and C.

Although, the general trend of the half-lives as calculated by Method C is very good, it should be pointed out that this calculation is somehow deceptive due to the negligence of the very important physical property of the bound state wavefunction. This property is taken into account in Method B through the physical concept of the zero point vibrational energy of equation (3.44). The excellent agreement of the half-lives as calculated in Method B with the measured values is thus not unexpected.

In Fig 5.10, we compare the logarithmic half-lives of the different models. It is seen that in the region of neutron deficient p-nuclei (i.e. the stable proton-rich nuclides that lie between ^{94}Se and ^{196}Hg on the chart of nuclides) the Methods agree quite well with the observed values. The discrepancy among the models is seen around the parent nucleons number $170 \sim 210$. The deviation of the half-lives as obtained from Method A is seen to come from mass number region 168 and beyond.

With the analyzed data, the quantitative agreement of the half-lives of Method B and C with experimental data is reasonable. The half-lives of the odd mass nuclei considered are well accounted for. The value of half-life of the nucleus ^{217}Th is underestimated by Method A possibly due to additional centrifugal contribution to the barrier. Another discrepancy among the methods is due to the shell and Pauli effects. In SAFM, however, the shell effects are implicitly contained in the zero point vibration energy due to its proportionality with the Q-value, which is maximum when the daughter nucleus has a magic number of neutrons and protons. Nonetheless, the values of $T_{1/2}$ for the nuclei ^{144}Nd, ^{146}Sm, ^{150}Gd and ^{152}Gd as calculated in Method B are underestimated. The change is possibly due to the factors mentioned above.

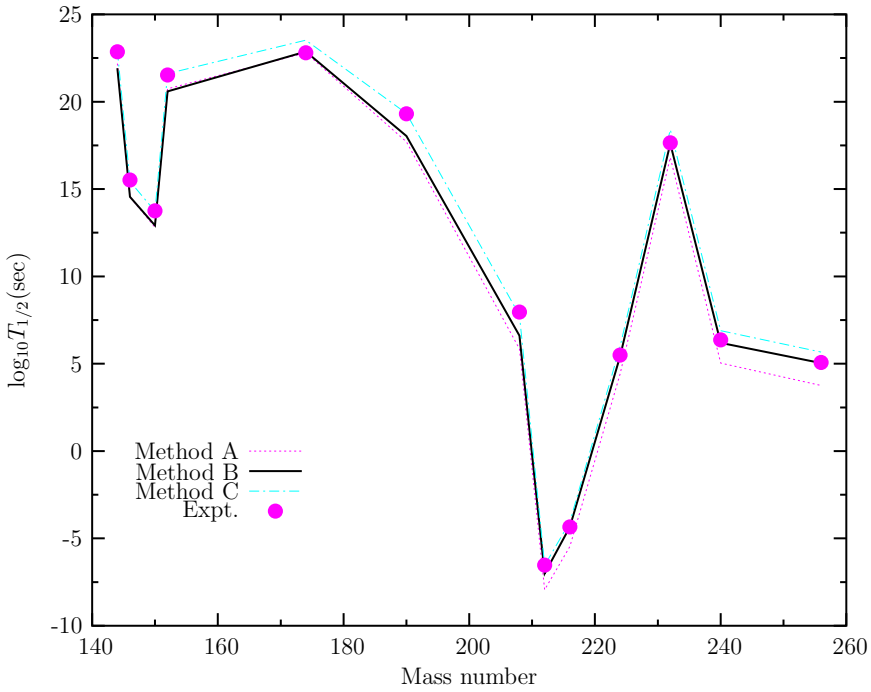

Figure 5.10: Logarithmic half-lives against parent mass number calculated with different models.

Chapter 6

Conclusions

In this thesis, we have tried to review the theoretical models available for numerical computation of spherical alpha decay nuclei and put forward the present status of the microscopic theories of alpha radioactivity. We think that the touchstone for a microscopic description is the absolute width. Our aim is to review theories rather than results, and that is why we focussed on models.

Three theories for describing the ground-state alpha radioactivity in spherical nuclei have been investigated: the quasi-bound state wavefunction approach, the superasymmetric fission model, and the quasiclassical method. In spite of the different degrees of sophistication in these models, they were nonetheless found to give rather similar results.

In this work, all of the models we studied heavily depend on a realistic α-nucleus potentials. The half-lives for α-decay have been analyzed with both microscopic (DFM) and optical nuclear potentials. The microscopic nuclear potentials are based on profound theoretical basis. It has been shown in Ref [78] that a systematic double folding potential is able to reproduce both the bound state properties and elastic α scattering of nuclei. It is worth mentioning that our calculations using realistic microscopic nuclear interaction potentials have been performed without adjusting the depth of the nuclear

potentials using any renormalization or adjusting any other parameters. Despite this, the results of these calculations i.e. SAFM and QCA using microscopic potentials are in excellent agreement over a small range of experimental data spanning about twelve orders of magnitude.

Using the SAFM model, we have tested our calculations by considering both the M3Y and DDM3Y effective NN interaction supplemented by a pseudo-potential. The results obtained are in good agreement with experimental data. Present calculations show that the differences in the results of the α-decay lifetimes obtained using the spherical charge distributions or point charge distributions for calculating the Coulomb interaction are small.

In the QSWA approach, we take into account the resonance nature of the quasistationary state using two sets of parameters of Woods-Saxon (WS) optical potential. The sensitivity of the calculated half-lives on variations in the optical potential parameters has been studied. Comparison with the experimental data, our results show that the WS potential with set A is preferable. Clearly, the results obtained from the two sets agree within an order of ~ 10, however, they both underestimate the observed values due to the highly correlated ambiguities between the parameters of the potentials. At the moment, no optical potential has been found to adequately account for α-decay half-lives. We conclude that we can find a better agreement to the experimental values if the WS optical potential is replaced with the more realistic DFM potential.

The final points to emerge from this study concern general trends in the behaviour of $(T_{1/2}^{calc}/T_{1/2}^{expt})$ which may reflect corresponding trends in the α-preformation factor P. Although we can adequately describe the α-decays of nuclei by all the methods, methods A and C, underestimate and overestimate the half-lives in a systematic manner, respectively. This can be corrected by adjusting the DFM potential strength parameter to the energy of the α-particle bound states wavefunction in the QCA model. In addition, there is an indication of a small systematic increase in P to the higher mass number as

the $N = 82$ neutron shell closure is approached as manifested by the decay data in Fig. 5.9.

Bibliography

[1] E. Roecki, Radiochim. Acta **70/71** (1995).

[2] G. Dodig-Crnković, F .A. Janouch, and R. J. Liotta, Phys. Lett. **B 139** (1984) 143; G. Dodig-Crnković, F .A. Janouch, and R. J. Liotta, and Z. Xiaolin, Phy. Scr. **37** (1988) 523.

[3] H. J. Rose, G. A. Jones, Nature **307** (1984) 245; D. V. Aleksandrov, A. F. Belyatskii, Yu. A. Glukhov, Yu. E. Nikol'skii, B. G. Novatskii, A. A. Oglobin, D. N. Stepanov, JETP Lett. **40** (1984) 909.

[4] H. J. Mang, Ann. Rev. Nucl. Sci. **14** (1964) 1

[5] W. Greiner, M. Ivaşcu, D. N. Poenaru and A. Săndulescu, in: D. A. Bromley (Editor), *Treatise on Heavy Ion Science* Vol.**8** (Plenum, New York), 1989, p. 641.

[6] G. Z. Gamow, Phys. **51** (1928) 204.

[7] E. U. Condon and R. W. Guerney, Nature **122** (1928) 439; Phys. Rev. **33** (1929) 127.

[8] E. Segre, *Nuclei and Particles* (W.A. Benjamin, Inc., Reading, Mass.) 1977 Chap. 7.

[9] M. A. Preston and R. K. Bhaduri, *Structure of the Nucleus* (Addison-Wesley Publishing Company, Mass.) 1975 Chap. 11.

[10] S. Rosenblum, J. Phys. Radium **1** (1930) 438.

[11] B. Buck, A. C. Merchant and S. M. Perez, Phys. Rev. Lett. **65** (1990) 2975; J. Phys. G: Nucl. Part. Phys. **17** (1991) 1223; **18** (1992) 143.

[12] B. Buck, A. C. Merchant and S. M. Perez, Phys. Rev. **C 45** (1992) 2247.

[13] B. Buck, A. C. Merchant and S. M. Perez, At. Data Nucl. Data Tables **54** (1993) 53.

[14] B. Buck, A. C. Merchant and S. M. Perez, Phys. Rev. **C 51** (1995) 559.

[15] S. A. Gurvitz and G. Kalbermann, Phys. Rev. Lett. **59** (1987) 262;
S. A. Gurvitz, Phys. Rev. **A 38** (1988) 1747.

[16] G. Breit, E. P. Wigner, Phys. Rev. **49** (1936) 519.

[17] R. G. Lovas, R. J. Loitta, A. Insolia, K. Varga, D. S. Delion, Phys. Rep. **294** (1998) 265.

[18] K. Varga, R. G. Lovas and R. J. Liotta, Phys. Rev. Lett. **69** (1992) 37; Nucl. Phys. **A 550** (1992) 421.

[19] R. G. Thomas, Prog. Theor. Phys. **12** (1954) 253.

[20] T. Teichmann, E. P. Wigner, Phys. Rev. **87** (1952) 123;

[21] H. J. Mang, Z. Phys. **148** (1957) 582; Phys. Rev. **119** (1960) 1069.

[22] I. Tonozuka, A. Arima, Nucl. Phys. **A 323** (1979) 45.

[23] A. Arima, S. Yoshida, Nucl. Phys. **A 219** (1974) 475.

[24] D. S. Delion, A. Florescu., M. Huyse, J. Wauters, P. Van Duppen, ISOLDE Collaboration, A. Insolia, R. J. Liotta, Phys. Rev. Lett. **74** (1995) 3939; D. S. Delion, A. Florescu., M. Huyse, J. Wauters, P. Van Duppen, ISOLDE Collaboration, A. Insolia, R. J. Liotta, Phys. Rev. **C 54** (1996) 1169.

[25] J. O. Rasmussen, Nucl. Phys. **44** (1963) 93.
J. O. Rasmussen, in: K. Siegbahn (Editor), *Alpha-, Beta- and Gamma-Ray Spectroscopy*, Vol. I, (North-Holland, Amsterdam) 1965, p. 701.

[26] T. Fliessbach, H. J. Mang, Nucl. Phys. **A 263** (1976) 75.

[27] F. A. Janouch and R. J. Liotta, Phys. Lett. **B 82** (1979) 329; Nucl. Phys. **A 334** (1980) 427.

[28] T. Steinmayer, W. Sünkel, K. Wildermuth, Phys. Lett. **B 125** (1983) 437.

[29] G. Dodig-Crnković, F. A. Janouch, R. J. Liotta and L. J. Sibanda, Nucl. Phys. **A 444** (1985) 419;
G. Dodig-Crnković, F. A. Janouch, R. J. Liotta, Nucl. Phys. **A 501** (1989) 533.

[30] A. Insolia, R. J. Liotta, E. Maglione, Europhys. Lett. **7** (1988) 209.

[31] S. Okabe, J. Phys. Soc. Japan Suppl. **58** (1989) 516.

[32] T. Fliessbach, Z. Phys. **A 272** (1975) 39.

[33] K. Harada, Prog. Theor. Phys. **26** (1961) 667.

[34] V. G. Soloviev, Phys. Lett. **1** (1962) 202.

[35] F. Catara, A. Insolia, E. Maglione, A. Vitturi, Phys. Rev. **C 29** (1984) 1091; Phys. Lett. **B 149** (1984) 41.

[36] A. Insolia, P. Curutchet, R. J. Liotta, D. S. Delion, Phys. Rev. **C 44** (1991) 545.

[37] F. A. Janouch and R. J. Liotta, Phys. Rev. **C 27** (1983) 896.

[38] K. Wildermuth, F. Fernandez, E. J. Kanellopoulos, W. Sünkel, J. Phys. **G 6** (1980) 603.

[39] K. Kaneko, M. Hasegawa, Phys. Rev. **C 67** (2003) 041306. M. Hasegawa, K. Kaneko, Phys. Rev. **C 61** (2000) 037306.

[40] I. Tomoda, A. Arima, Nucl. Phys. **A 303** (1978) 217.

[41] R. J. Liotta and C. Pomar, Nucl. Phys. **A 382** (1982) 1.

[42] J. K. Poggenburg, H. J. Mang, J. O. Rasmussen, Phys. Rev. **181** (1969) 1697.

[43] D. S. Delion, A. Insolia, R. J. Liotta, Phys. Rev. **C 46** (1992) 848; Phys. Rev. **C 46** (1992) 1346; Phys. Rev. **C 49** (1994) 3024.

[44] D. S. Delion, A. Insolia, and R. J. Liotta, Nucl. Phys. **A 549** (1992) 407.

[45] K. Harada, E. A. Rauscher, Phys. Rev. **169** (1968) 818.

[46] S. G. Kadmenskiĭ, V. E. Kalechits, Sov. J. Nucl. Phys. **12** (1971) 71; V. I. Furman, S. Holan, S. G. Kadmenskiĭ, G. Stratan, Nucl. Phys. **A 226** (1974) 131.

[47] J. Schlitter, Nucl. Phys. **A 211** (1973) 96.

[48] M. Goldberger and K. M. Watson, *Collision Theory* (Wiley, New York, N.Y.) 1964.

[49] A. Săndulescu, I. Silişteanu, R. Wünsch, Nucl. Phys. **A 305** (1978) 205.

[50] H. Feshbach, Ann. Phys. (N.Y.) **5** (1958) 357; **19** (1962) 287.

[51] D. F. Jackson, M. Rhoades-Brown Ann. Phys. (N.Y.) **105** (1977) 151.

[52] K. Wildermuth, Y. C. Yang, *A Unified Theory of the Nucleus* (Academic, New York) 1977.

[53] A. Săndulescu, D. N. Poenaru, W. Greiner, Sov. J. Part. Nucl. **11** (1980) 528.

[54] D. N. Poenaru, M. Ivaşcu, J. Phys. (France) **45** (1984) 1099;
D. N. Poenaru, M. Ivaşcu, A. Săndulescu, W. Greiner, J. Phys. G: Nucl. Phys. **10** (1984) L183.

[55] D. N. Poenaru, W. Greiner, K. Depta, M. Ivaşcu, D. Mazilu and A. Săndulescu, At. Data Nucl. Tables **34** (1986) 423.

[56] D. N. Poenaru, D. Schnabel, W. Greiner, D. Mazilu and R. Gherghescu, At. Data Nucl. Tables **48** (1991) 231.

[57] S. S. Malik, R. K. Gupta, Phys. Rev. **C 39** (1989) 1992.

[58] D. N. Basu, Phys. Rev. **C 66** (2002) 027601; Phys. Lett. **B 566** (2003) 90.

[59] D. N. Basu, J. Phys. G: Nucl. Part. Phys. **30** (2004) B35.

[60] K. S. Krane, *Introductory Nuclear Physics.* (Wiley, New York, N.Y.) 1987.

[61] D. S. Delion and R. J. Liotta, Phys. Rev. **C 58** (1998) 2073.

[62] D. S. Delion and A. Săndulescu, J. Phys. G: Nucl. Part. Phys. **28** (2002) 617.

[63] D. S. Delion, A. Insolia, R. J. Liotta, Phys. Rev. **C 54** (1996) 407.

[64] M. Ivaşcu, I. Silişteanu, Nucl. Phys. **A 485** (1988) 93.

[65] D. N. Basu, J. Phys. G: Nucl. Part. Phys. **29** (2003) 2079.

[66] Y. K. Gambhir, A. Bhagwat, M. Gupta and Arun K. Jain, Phys. Rev. **C 68** (2003) 044316.

[67] A. M. Kobos, B. A. Brown, R. Lindsay and G. R. Satchler Nucl. Phys. **A 425** (1984) 205.

[68] G. R. Satchler and W. G. Love, Phys. Rep. **55** (1979) 183; Dao. T. Khoa, Phys. Rev. **C 63** (2001) 034007.

[69] Dao. T. Khoa, W. von Oertzen and H. G. Bohlen, Phys. Rev. **C 49** (1994) 1652; M. E. Brandan and G. R. Satchler, Phys. Rep. **285** (1997) 143.

[70] Dao. T. Khoa and G. R. Satchler, Nucl. Phys. **A 668** (2000) 3.

[71] Dao. T. Khoa and W. von Oertzen, Phys. Lett. **B 304** (1993) 8; Dao. T. Khoa, G. R. Satchler and W. von Oertzen, Phys. Rev. **C 56** (1997) 954.

[72] A. K. Chaudhuri, Nucl. Phys. **A 449** (1986) 243.

[73] J. Cook, Comput. Phys. Commun. **25** (1982) 125.

[74] K. Wildermuth and W. Mac Clure, *Cluster Representation of Nuclei* (Berlin–Heidelberg–New York: Springer) 1966.

[75] G. Audi and A. H. Wapstra, Nucl. Phys **A 595** (1995) 409.

[76] L. McFadden and G. R. Satchler, Nucl. Phys. **84** (1966) 177.

[77] D. N. Basu, Private Communication.

[78] U. Atzrott, P. Mohr, H. Abele, C. Hillenmayer and G. Staudt, Phys. Rev. **C 53** (1996) 1336.